AGU PUBLICATIONS

Tectonics

RESEARCH ARTICLE
10.1002/2014TC003637

Key Points:
- Nadanhada Terrane is an accretionary complex
- Basaltic rocks have OIB and N-MORB affinities
- Onset of Pacific accretion at 210–180 Ma, final emplacement at 137–130 Ma

Correspondence to:
J.-B. Zhou,
zhoujianbo@jlu.edu.cn

Citation:
Zhou, J.-B., J.-L. Cao, S. A. Wilde, G.-C. Zhao, J.-J. Zhang, and B. Wang (2014), Paleo-Pacific subduction-accretion: Evidence from Geochemical and U-Pb zircon dating of the Nadanhada accretionary complex, NE China, *Tectonics*, *33*, 2444–2466, doi:10.1002/2014TC003637.

Received 4 JUN 2014
Accepted 20 OCT 2014
Accepted article online 24 OCT 2014
Published online 13 DEC 2014

Paleo-Pacific subduction-accretion: Evidence from Geochemical and U-Pb zircon dating of the Nadanhada accretionary complex, NE China

Jian-Bo Zhou[1], Jia-Lin Cao[1], Simon A Wilde[1,2], Guo-Chun Zhao[3], Jin-Jiang Zhang[4], and Bin Wang[1]

[1]College of Earth Sciences, Jilin University, Changchun, China, [2]Department of Applied Geology, Curtin University, Perth, Western Australia, Australia, [3]Department of Earth Sciences, University of Hong Kong, Hong Kong, China, [4]Department of Geology, Peking University, Beijing, China

Abstract The Nadanhada Terrane, located along the eastern margin of Eurasia, contains a typical accretionary complex related to paleo-Pacific plate subduction-accretion. The Yuejinshan Complex is the first stage accretion complex that consists of meta-clastic rocks and metamafic-ultramafic rocks, whereas the Raohe Complex forms the main parts of the terrane and consists of limestone, bedded chert, and mafic-ultramafic rocks embedded as olistolith blocks in a weakly sheared matrix of clastic meta-sedimentary rocks. Geochemical data indicate that the Yuejinshan metabasalts have normal mid-ocean ridge basalt (N-MORB) affinity, whereas the Raohe basaltic pillow lavas have an affinity to ocean island basalts (OIB). Sensitive high-resolution ion microprobe (SHRIMP) U-Pb zircon analyses of gabbro in the Raohe Complex yield a weighted mean $^{206}Pb/^{238}U$ zircon age of 216 ± 5 Ma, whereas two samples of granite intruded into the complex yield weighted mean $^{206}Pb/^{238}U$ zircon ages of 128 ± 2 and 129 ± 2 Ma. Laser ablation inductively coupled plasma mass spectrometry (LA-ICPMS) U-Pb zircon analyses of basaltic pillow lava in the Raohe Complex define a weighted mean age of 167 ± 1 Ma. Two sandstone samples in the Raohe Complex record younger concordant zircon weighted mean ages of 167 ± 17 and 137 ± 3 Ma. These new data support the view that accretion of the Raohe Complex was between 170 and 137 Ma, and that final emplacement of the Raohe Complex took place at 137–130 Ma. The accretion of the Yuejinshan Complex probably occurred between the 210 and 180 Ma, suggesting that paleo-Pacific plate subduction was initiated in the Late Triassic to Early Jurassic.

1. Introduction

Northeast China and adjacent regions of the Russian Far East, South Korea, and central southwest Japan developed geologically by the collision of micro-continental blocks in the Phanerozoic. Two major tectonic belts have been distinguished (Figure 1). The western part includes the Songliao, Xing'an, and Erguna blocks, which together form part of the Central Asian Orogenic Belt (CAOB), marking the broad collision zone between the North China and Siberia cratons. These areas contain mélange, Paleozoic syn-collisional granitoids, and Mesozoic post-orogenic A-type granites [*Sengör et al*., 1993; *Sengör and Natal'in*, 1996; *Wu et al*., 2002, 2011; *Xiao et al*., 2003, 2004a, 2004b; *Windley et al*., 2007; *Zhou et al*., 2011a, 2011b, 2012a; *Zhou and Wilde*, 2013; *Kröner et al*., 2014]. The eastern part, including the Jiamusi, Khanka, Bureya, and Nadanhada terranes of NE China, the Sikhote-Alin Terrane of the Russian Far East, and the Japanese islands (Figures 1 and 2a), belong to the Pacific margin and are characterized by Mesozoic subduction complexes, large-scale NE-trending granite and volcanic belts, and wrench fault systems [*Xu et al*., 1987; *Tang*, 1990; *Faure and Natal'in*, 1992; *Ren et al*., 1999a, 1999b; *Natal'in*, 1991, 1993; *Maruyama*, 1997; *Wilde et al*., 2000, 2003; *Wu et al*., 2011; *Zhou et al*., 2009, 2010a, 2010b, 2010c; *Zhou and Wilde*, 2013]. The Nadanhada Terrane (or accretionary complex) is a key area for understanding the processes of paleo-Pacific subduction-accretion since the Mesozoic.

The Nadanhada Terrane (Figures 1, 2a and 2b) is situated at the boundary between the Russian Far East and NE China, and was previously considered to be either part of the paleo-Pacific subduction zone or an exotic terrane [*Li et al*., 1979; *Shao et al*., 1990, 1991; *Shao and Tang*, 1995; *Mizutani et al*., 1989; *Mizutani and Kojima*, 1992; *Kojima and Mizutani*, 1987; *Kojima*, 1989; *Zhou et al*., 2009]. The occurrence of Triassic-Jurassic radiolarians in the Nadanhada Terrane has been known since the 1950s [*Wang*, 1959; *Li et al*., 1979; *Mizutani et al*., 1989; *Kojima and Muzutani,* 1987; *Kojima*, 1989; *Zhang*, 1990]. Primarily, on the basis of the radiolarian

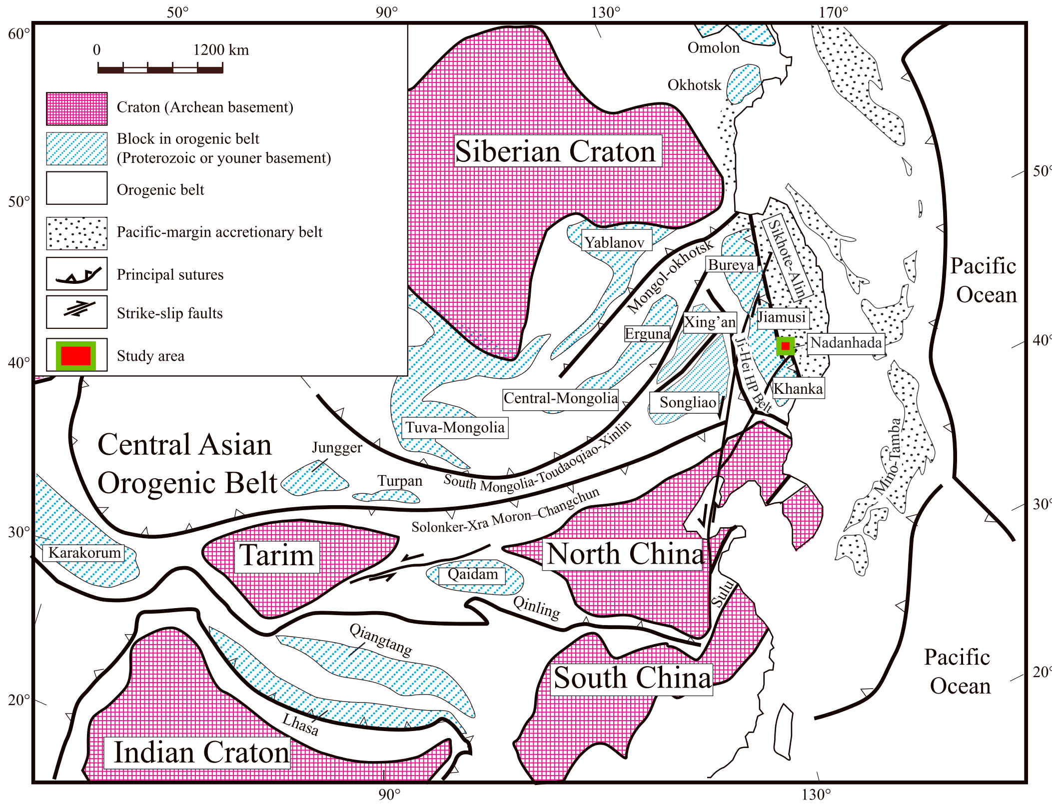

Figure 1. Schematic tectonic map showing the main subdivisions of central and eastern Asia and location of the study area (modified from *Zhou et al.*, 2009).

studies, the Nadanhada Terrane has been considered as an ophiolitic mélange that contains some tectonic lenses of Carboniferous to Permian limestone and greenstone (mafic-ultramafic sequences), Triassic-Middle Jurassic bedded chert, and siliceous shale, all enclosed in post-Middle Jurassic clastic rocks [*Wang*, 1959; *Li et al.*, 1979; *Mizutani et al.*, 1989; *Kojima and Mizutani*, 1987; *Kojima*, 1989; *Zhang*, 1990; *Ding et al.*, 1997]. *Mizutani et al.* [1989] and *Kojima* [1989] suggested that the Nadanhada Terrane in NE China, the Sikhote-Alin Terrane in the Russian Far East, and the Mino-Tamba Terrane in central Japan comprise parts of a Mesozoic superterrane situated originally at the northwest margin of the Pacific Ocean and continuously accreted to the eastern continental margin of Eurasia in the Mesozoic. The Nadanhada and Sikhote-Alin terranes are juxtaposed, but the central Japan Terrane is now separated by the Japan Sea that was opened in the Neogene time [*Mizutani et al.*, 1989; *Mizutani and Kojima*, 1992; *Kojima and Mizutani*, 1987; *Kojima*, 1989; *Zhang*, 1990; *Zhang et al.*, 1997; *Cheng et al.*, 2006; *Zyabrev and Matsuoka*, 1999]. The Nadanhada Terrane contains mafic-ultramafic sequences, including basaltic pillow lavas, gabbros, and ultramafic cumulate rocks including wehrlite, clinopyroxenite, and minor lherzolite and websterite [*Cui*, 1986; *Kang et al.*, 1990]. Chromite deposits also occur in the Hamatong and Hongqishan areas (Figure 2b). A few geochemical and geochronological studies were focused on the basalt in order to identify the nature of the mafic-ultramafic sequences [*Cui*, 1986; *Kang et al.*, 1990; *Zhang and Zhou*, 2001; *Shao and Tang*, 1995; *Cheng et al.*, 2006]. Most workers suggest that the mafic-ultramafic rocks are ophiolitic sequences associated with radiolarian-bearing chert and shale [*Mizutani et al.*, 1989; *Mizutani and Kojima*, 1992; *Cui*, 1986; *Kojima and Mizutani*, 1987; *Kojima*, 1989; *Kang et al.*, 1990; *Zhang and Mizutani*, 2004; *Shao et al.*, 1990, 1991; *Shao and Tang*, 1995]. However, *Zhang and Zhou* [2001] concluded that these mafic-ultramafic rocks did not originate at a mid-ocean ridge or supra-subduction zone but formed in a seamount setting. *Ishiwatari and Ichiyama* [2004] also argued that these mafic-ultramafic rocks are not ophiolite but were intruded into the Jurassic chert-shale-sandstone sequences, and formed as the result of a superplume in or near the subduction zone. In summary, most previous studies have focused on the paleobiological data, and there is a lack of high-quality geochemical and geochronological data; thus, the protolith nature and tectonic setting of the Nadanhada Terrane remain unclear.

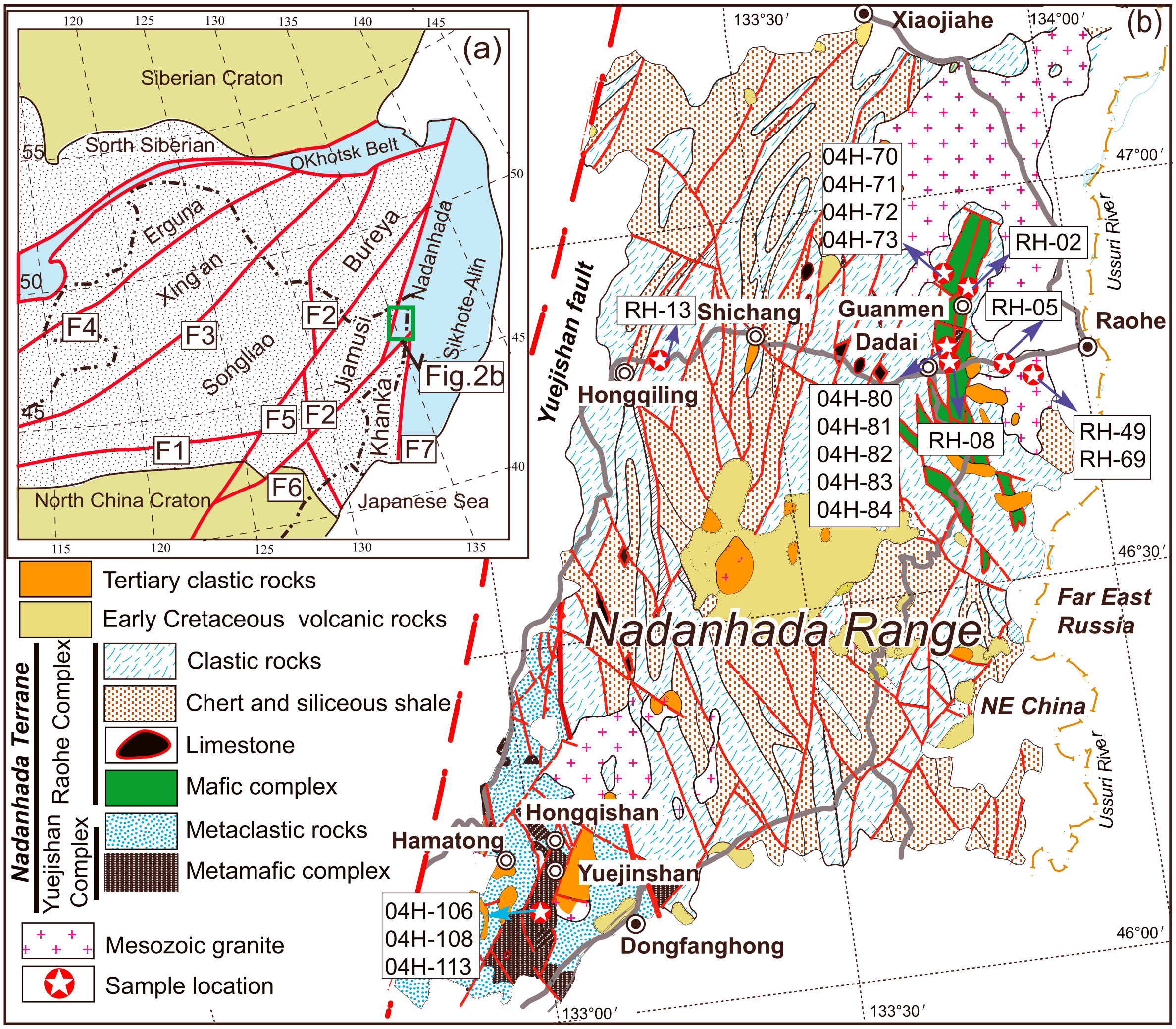

Figure 2. (a) Geological sketch map of NE China and adjacent areas [after *Zhou et al.*, 2011a, 2011b]. F1 = Solonker-Xar Moron-Changchun suture; F2 = Jilin-Heilongjiang high-pressure metamorphic belt; F3 = Hegenshan-Heihe suture; F4 = Xinlin-Xiguitu suture; F5 = Yilan-Yitong Fault; F6 = Dunhua-Mishan Fault, and F7 = Primoria Fault. (b) Detailed geological map of the Nadanhada Terrane showing sample locations (after HBGMR, 1987).

In this paper, we present geochemical and both sensitive high-resolution ion microprobe (SHRIMP) and laser ablation inductively coupled plasma mass spectrometry (LA-ICPMS) U-Pb zircon data for the Nadanhada Terrane. These data will enable evaluation of the nature and age of the protolith, and also allow us to place constraints on the timing of emplacement of the Nadanhada Terrane. These results will provide further insight into the tectonic setting of the Nadanhada Terrane with respect to paleo-Pacific subduction-accretion.

2. Regional Setting

The eastern part of NE China consists of a collage of several micro-continental blocks or terranes [*Tang*, 1990; *Li*, 2006; *Zhou and Wilde*, 2013], including the Nadanhada Terrane in the northeast, the Songliao-Zhangguangcai block in the southwest, and the Jiamusi-Khanka Block in the central part, separated by the Mudanjiang and Yuejinshan Faults (Figure 2a).

The Nadanhada Terrane is located to the east of the Jiamusi Block and forms part of the paleo-Pacific accretion belt, being mainly composed of Triassic-Jurassic accretionary complexes that were intruded by Cretaceous granites [*Kojima*, 1989; *Cheng et al.*, 2006]. The Triassic-Jurassic accretionary complexes of the Nadanhada Terrane are broadly divided into two major lithostratigraphic units based on field occurrence as shown on the 1:200,000 geological map [*Heilongjiang Bureau of Geology and Mineral Resources (HBGMR)*,

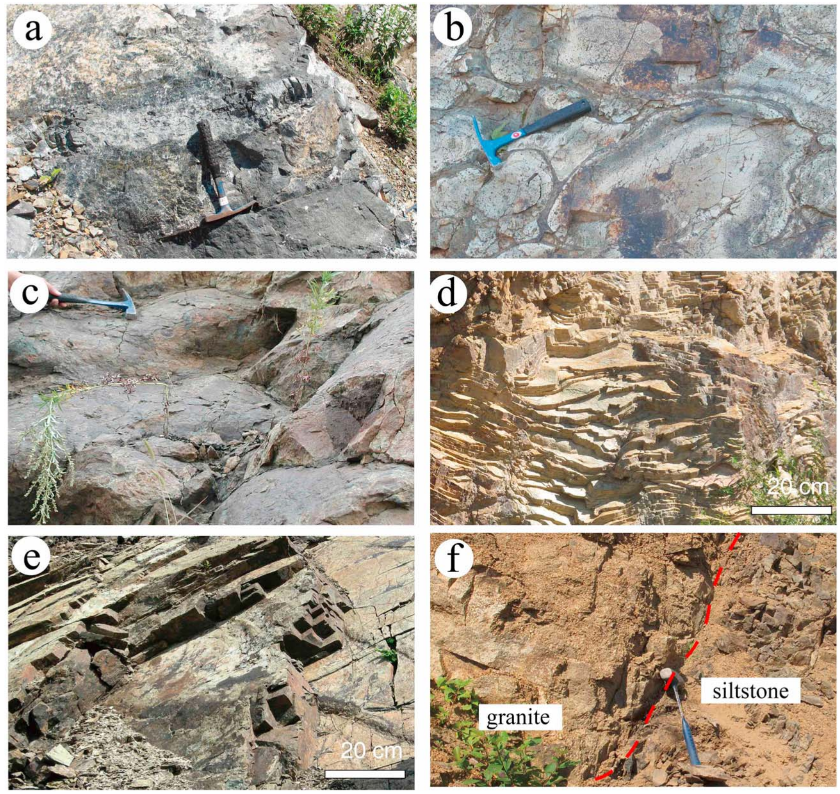

Figure 3. Field photographs of the Nadanhada Terrane. (a) Location of gabbro sample RH-02 showing cumulate textures. (b) Location of basalt samples 04H(71–73) showing pillow structures. (c) Location of basalt samples 04H(80–84) and RH-08 showing pillow structures. (d) Bedded chert displaying intra-formational folds. (E) Location of thick-bedded sandstone sample RH-13; and (F) Location of siltstone sample RH-05 in contact with Mesozoic granite.

1987]: the Yuejinshan and Raohe complexes. The Yuejinshan Complex is the first stage accretion complex and only occurs in the Yuejinshan area, whereas the Raohe Complex constitutes the main part of the terrane and consists of a typical tectonic mélange (Figure 2b).

2.1. Yuejinshan Complex

The Yuejinshan Complex lies at the western edge of the Nadanhada Terrane and is separated by the Yuejinshan Fault from the Jiamusi Block (Figure 2b); it was previously referred to as the Yuejinshan “Group” in the Chinese literature. The Yuejinshan Complex consists mainly of units of meta-clastic rocks and mafic-ultramafic rocks (Figure 2b). The meta-clastic rocks include quartzite, quartz-schist, marble, two-mica schist, and quartz-mica-schist, and are interpreted as continental slope sediments that experienced lower greenschist-facies metamorphism [*Zhang et al.*, 1997; *Zhang and Zhou*, 2001; *Yang et al.*, 1998]. The mafic-ultramafic rocks comprise typical ophiolitic sequences of metabasalts, gabbro, and ultramafic rocks including dunite, wehrlite, and clinopyroxenite, with extensive chromite deposits in the Hamatong and Hongqishan areas (Figure 2b). The Yuejinshan Complex was considered Middle Paleozoic in age [*HBGMR*, 1987, 1993]. However, *Zhang et al.* [1997] pointed out that the meta-clastic rock unit consists of Triassic-Early Jurassic sediments and that timing of emplacement should be after the Early Jurassic. *Yang et al.* [1998] further reported a whole-rock Rb-Sr age of 188 ± 4 Ma for greenschist of the Yuejinshan Complex in the Dongfanghong area, indicating that the Yuejinshan Complex was metamorphosed in the Early Jurassic.

2.2. Raohe Complex

The Raohe Complex forms the main part of the Nadanhada Terrane, and is located at the boundary between the Russian Far East and NE China (Figure 2b). It is composed of four units [*Kojima and Mizutani*, 1987; *Kojima*, 1989; *Zhang and Mizutani*, 2004; *Cheng et al.*, 2006]: limestone, mafic-ultramafic rocks, chert and siliceous shale, and clastic rocks. The mafic-ultramafic rocks are well exposed in areas about 50 km long and 5–8 km in width from Guanmen to Dadai. They occur as tectonic lenses in post-Middle Jurassic clastic rocks, as pyroxene peridotite, pyroxenite, gabbro, and dolerite dykes, with distinct cumulate textures (Figure 3a). *Cui* [1986] reported komatiite showing spinifex texture, but this has yet to be substantiated. The basalts with pillow structures (Figures 3b and 3c) are amygdaloidal and invariably altered. The limestone mainly outcrops in the Shichang and Hongqiliang areas (Figure 2b), and is up to 10 m thick and embedded as olistoliths in a weakly sheared clastic matrix [*Mizutani et al*., 1989]. The limestone is massive, homogeneous and gray in color. *Li et al*. [1979] reported Middle Carboniferous fusulinids and corals from the limestone, whereas *Wang et al*. [1986] reported upper Triassic conodonts from bedded limestone within chert interbands near Hongqiling. The chert and siliceous shale invariably display intra-formational folds (Figure 3d) and comprise isolated blocks enclosed in a clastic matrix. The size of these chert blocks ranges from 20 to 100 m, and they show rhythmic bedding of ~5 cm thick chert with thinner shale partings. Middle to Late Triassic radiolarian fossils were extracted from bedded chert, and Middle Jurassic radiolarians were extracted from siliceous shale in the Nadanhada Terrane [*Kojima and Mizutani*, 1987]. The clastic rocks consist of a mixed assemblage that includes graywacke, sandstone (Figure 3e), siltstone (Figure 3f), and mudstone, which was considered to be "matrix" and of post-Middle Jurassic age [*Kojima and Mizutani*, 1987; *Kojima*, 1989; *Shao et al*., 1990].

3. Sample Locations and Descriptions

3.1. Basaltic Pillow Lava From the Raohe Complex

Ten samples of basaltic pillow lava were collected from mafic-ultramafic rocks of the Raohe Complex. Samples 04H-70, 71, 72, and 73 were collected at Guanmen, ~22 km NW of Raohe (N46°54′18.4″ E133°46′47.5″; Figures 2b and 3b), and samples RH-08; 04H-80, 81, 82, 83, and 84 were collected at Dadai (N46°47′47.8″ E133°45′42.1″; Figures 2b and 3c), ~15 km west of Raohe, where they occur as a tectonic lenses in sandstone. They show well-developed pillow structures, 0.2–0.5 m in width and ~0.4–0.8 m long (Figures 3b and 3c), indicating a subaqueous volcanic origin. The texture of the pillow lava varies between sub-ophitic, porphyritic, and seriate, with total phenocryst contents ranging from 10 to 20%. The lavas generally contain phenocrysts of plagioclase (50%), titanaugite (30%), and olivine (15%) set in a fine-grained groundmass of granular olivine, plagioclase laths, and intersertal glass. Other primary phases include ilmenite and titanium-rich magnetite. Some glassy rocks have phenocrysts of equant to elongate-skeletal olivine with included or attached oxide phases, set in a dark brown glass. Secondary minerals include chlorite, calcite, epidote, and titanite.

3.1.2. Cumulate Gabbro From the Raohe Complex

Sample RH-02 was collected from Guanmen, ~20 km NW of Raohe (N46°52′58.9″ E133°48′59.4″; Figures 2b and 3a). It has distinct cumulate textures and displays phase and rhythmic layering. Some gabbros are medium to coarse grained with a granular allotriomorphic texture composed of clinopyroxene (30–33%) and plagioclase (60–63%), both ranging in size from 0.5 to 5 mm, plus fine-grained olivine (3–5%; 0.25–2 mm) and sparse spinel. Medium-grained gabbro is composed of plagioclase (50–70%), clinopyroxene (15–25%), with or without olivine ($\leq$5%), interstitial Fe-Ti oxides (10–15%), and accessory amounts of brown amphibole and apatite.

3.2. Granite

Granite samples RH-49 and RH-69 were collected ~6 km west of Raohe (N46°47′25″ E133°51′47.2″, Figure 2b), where a granite pluton crops out for $>$700 km^2 and intrudes the Raohe Complex (Figure 3f). The sample is composed of plagioclase (35%–40%), K-feldspar (25–33%), quartz (25–30%), biotite (5–6%), and cordierite ($<$5%), with minor amounts of apatite, titanite, zircon, ilmenite, and secondary limonite. Magmatic cordierite is commonly found in the Raohe granite, which shows peraluminous characteristics, indicating an S-type affinity [*Cheng et al*., 2006].

3.3. Metabasalts From the Yuejinshan Complex

Samples 04H-106, 108, and 113 are metabasalts collected along the road side from the Dongfanghong to Hongqishan chromite deposits of the Yuejinshan Complex (Figure 2b). Pillow lavas are locally present, but the majority of the basalts are massive. Both plagioclase-phyric and aphyric types are common, and they have a greenish tint due to the presence of secondary chlorite and serpentine. The basalts are composed of plagioclase, clinopyroxene, and opaque minerals that are variably replaced by sericite, calcite, clay minerals, serpentine, and chlorite. Quartz and calcite veins are common.

4. Analytical Methods

4.1. Major and Trace Elements

Analyses of major element oxides and trace elements, including rare earth elements (REE), were carried out at the Analytical Institute of the Hubei Bureau of Geology and Mineral Resources, Wuhan. Major elements were measured by XRF using a Regaku 3080E1 spectrometer. The analytical uncertainties are usually better than 0.3% to 0.9% for major elements. For REE and Nb, Ta, Zr, Hf, Th, and Ba, the samples were digested by alkaline-fusion and analyzed by JY48/JY38P ICP-AES at the same institute in Wuhan. The analytical uncertainties are better than 5% (2σ) for REE, and <10% for other trace elements. Analyses of international standard reference samples from this laboratory were reported in *Zhou et al*. [2012b].

4.2. SHRIMP U-Pb Determinations

One sample of gabbro (RH-02) and two samples of granite (RH-49 and RH-69) from the Raohe Complex were processed by crushing, followed by initial heavy liquid and subsequent magnetic separation techniques to concentrate the zircon crystals. Samples were divided into different size and magnetic fractions using an isodynamic separator. Zircons from the non-magnetic fractions were handpicked and mounted, along with pieces of the CZ3 zircon standard, onto double-sided adhesive tape, enclosed in epoxy resin, and then polished to about half their thickness. The mount was then cleaned and gold-coated and photographed in reflected and transmitted light. Cathodoluminescence (CL) images of zircon grains were obtained using a Philips XL30 scanning electron microscope (SEM) at Curtin University. U-Th-Pb analyses were conducted using a WA Consortium SHRIMP II ion microprobe housed at Curtin University, utilizing six-cycle runs through the mass stations. Detailed analytical procedures are described by *Nelson* [1997] and *Williams* [1998]. Isotopic ratios were monitored by reference to Sri Lankan gem zircon standard (CZ3) with a ^{206}Pb/^{238}U ratio of 0.0914 and a ^{206}Pb/^{238}U age of 564 Ma. Pb/U ratios in the unknown zircons were corrected using the ln (Pb/U)/ln (UO/U) relationship as measured on CZ3. All ages have been calculated from the U and Th decay constants recommended by *Steiger and Jäger* [1977]. Reported ages represent ^{206}Pb/^{238}U data that have been corrected using the measured ^{204}Pb [*Compston et al*., 1984]. The analytical data were reduced, calculated, and plotted using the Squid (1.0) and Isoplot/Ex_ver3 programs [*Ludwig*, 2003]. Individual analyses in the data table and on concordia plots are presented with 1σ error, and uncertainties in weighted mean ages are quoted at the 95% confidence level (2σ), unless otherwise indicated.

4.3. LA-ICPMS U-Pb Determinations

The zircon U-Pb dating and trace element analyses of samples RH-05, RH-08, and RH-13 were performed simultaneously by LA-ICP-MS at the State Key Laboratory of Geological Processes and Mineral Resources, China University of Geosciences, Wuhan. Detailed operating conditions for the LA-ICP-MS and data reduction procedures are the same as those described by *Liu et al*. [2008, 2010]. Laser ablation was performed using a GeoLas 2005 system, which was coupled to an Agilent 7500a ICP MS. Helium was used as the carrier gas and argon was mixed with this via a T-connector before entering the ICP MS plasma source. Nitrogen was added into the central gas flow (Ar + He) of the Ar plasma in order to improve the detection limits and precision [*Hu et al*., 2008]. Each U-Pb analysis incorporated a background measurement of approximately 20–30 s (gas blank) followed by 50 s of data acquisition.

An Agilent Chemstation was utilized for the acquisition of each analysis. Offline selection and integration of background and analyte signals, time-drift corrections, and quantitative calibration of trace element analyses and U-Pb dates were performed using the in-house software ICPMSDataCal [*Liu et al*., 2008, 2010].

Standards 91500, BCR-2G, and BIR-1G were mounted on the same mount as the unknowns for analysis. Zircon 91500 was used as the external standard for U-Pb dating, and was analyzed twice every five analyses. Time-dependent drift of U-Th-Pb isotopic ratios was corrected using a linear interpolation with time for every five analyses according to the variations measured for 91500 (i.e., two 91500 analyses + five sample analyses + two 91500 analyses) [*Liu et al*., 2010]. Preferred U-Th-Pb isotopic ratios used for 91500 were taken from *Wiedenbeck et al*. [1995]. Common Pb correction of the samples was calculated using ComPbCorr#3.17 [*Andersen*, 2003]. Uncertainties in the values for the external standard 91500 were propagated through the

Table 1. Major Element, Rare Earth Elements (REE), and Trace Element Analyses of Mafic Volcanic Rocks From the Nadanhada Terrane

	Raohe Complex Pillow Lava									Yuejinshan Complex Meta-Basalt		
Sample no	04H-70	04H-71	04H-72	04H-73	04H-80	04H-81	04H-82	04H-83	04H-84	04H-106	04H-108	04H-113
SiO_2	51.70	50.93	48.46	51.06	48.82	48.86	49.43	49.00	49.18	45.67	50.23	47.78
TiO_2	2.78	3.39	3.00	3.34	3.03	2.47	2.49	2.42	2.49	1.40	1.21	1.64
Al_2O_3	12.14	13.77	12.27	13.96	12.00	10.62	10.55	10.48	10.63	16.99	15.76	13.93
Fe_2O_3	3.04	3.78	3.38	3.27	3.48	3.55	3.04	3.28	3.62	4.70	3.54	7.54
FeO	7.98	9.15	8.95	7.48	10.12	8.08	8.70	8.35	8.23	7.65	6.92	6.20
MnO	0.15	0.21	0.19	0.16	0.19	0.17	0.16	0.17	0.17	0.22	0.18	0.24
MgO	5.68	3.65	6.48	4.58	7.43	9.29	9.41	9.32	9.32	4.93	4.47	4.67
CaO	10.49	9.22	11.34	9.16	7.45	9.76	8.92	9.64	9.33	10.89	8.47	12.57
Na_2O	3.54	3.15	2.67	3.95	3.07	2.96	2.92	2.90	2.98	1.90	2.74	2.00
K_2O	0.30	0.47	0.75	0.79	0.16	0.09	0.20	0.16	0.11	0.31	0.52	0.20
P_2O_5	0.34	0.59	0.35	0.48	0.35	0.27	0.28	0.27	0.30	0.16	0.11	0.15
Loss on Ignition (LOI)	0.73	0.41	0.86	0.68	2.48	2.68	2.63	2.78	2.45	4.12	4.88	2.15
Total	98.87	98.72	98.7	98.91	98.58	98.8	98.73	98.77	98.81	98.94	99.03	99.07
Rb	6	12	14	13	6	4	6	5	5	10	13	6
Sr	218	552	466	282	264	255	306	332	204	212	282	322
Ba	116.0	172.0	310.0	300.0	64.0	51.4	59.2	61.1	44.8	42.0	52.3	73.8
Nb	29.30	34.30	29.50	43.50	29.60	21.40	24.90	25.00	23.90	1.73	2.84	8.24
Ta	1.79	2.70	1.75	2.58	1.86	1.53	1.46	1.53	1.45	0.14	0.24	0.46
Zr	195	311	208	271	211	172	177	169	174	75	71	92
Hf	4.40	6.70	5.40	7.70	4.60	3.40	4.30	3.60	4.00	2.00	2.10	2.60
V	301	343	325	321	306	275	255	263	266	359	304	303
Th	3.84	5.18	2.69	4.00	2.35	1.51	1.89	2.16	1.98	1.44	1.37	1.01
U	0.87	0.81	0.51	0.86	0.28	0.47	0.45	0.39	0.38	0.14	0.13	0.41
Cr	237	15.1	252	89.7	372	634	595	620	579	189	164	134
Sc	30.6	22.6	29.5	23.8	30.9	30.9	26.6	32.1	27.9	44.5	45.3	43.8
Ni	83	22	83	66	152	256	238	260	251	58	50	50
Co	37	32	37	32	42	44	41	43	45	34	34	39
Y	27.94	35.74	30.42	27.60	41.88	21.27	22.19	21.76	21.98	40.99	31.95	42.99
La	21.42	36.70	23.79	35.15	40.09	19.31	19.64	18.69	23.91	3.35	2.30	3.95
Ce	43.82	82.46	50.93	70.12	69.14	41.53	42.50	39.52	45.77	10.24	6.94	11.05
Pr	6.44	11.09	7.38	9.98	8.69	6.21	6.40	5.93	6.71	2.19	1.33	2.03
Nd	28.51	48.38	32.32	40.42	32.13	26.13	26.51	25.53	28.33	12.01	7.71	11.07
Sm	6.35	10.35	7.07	8.62	6.15	5.88	6.03	5.91	6.13	4.53	2.92	3.92
Eu	2.16	3.00	2.49	2.77	1.96	1.94	1.97	1.96	2.09	1.74	1.17	1.50
Gd	6.50	9.51	7.36	8.19	6.01	6.05	6.03	5.98	6.22	6.31	4.25	5.84
Tb	1.03	1.43	1.15	1.28	0.90	0.93	0.96	0.95	0.97	1.15	0.82	1.12
Dy	5.46	7.72	6.16	6.74	5.14	5.16	5.27	5.13	5.34	7.44	5.45	7.47
Ho	0.99	1.37	1.12	1.23	0.97	0.95	0.95	0.91	0.98	1.54	1.17	1.61
Er	2.42	3.36	2.79	2.93	2.58	2.42	2.44	2.32	2.42	4.35	3.45	4.72
Tm	0.33	0.48	0.41	0.40	0.37	0.35	0.34	0.34	0.33	0.66	0.54	0.75
Yb	1.96	2.70	2.28	2.27	2.07	1.93	1.90	1.89	1.94	4.00	3.41	4.84
Lu	0.29	0.37	0.33	0.31	0.30	0.28	0.27	0.27	0.28	0.57	0.49	0.74
ΣREE	128	219	146	190	177	119	121	115	131	60	42	61
L/H	5.73	7.13	5.74	7.15	8.62	5.59	5.67	5.48	6.11	1.31	1.14	1.24
(La/Yb)n	7.84	9.75	7.48	11.11	13.89	7.18	7.41	7.09	8.84	0.60	0.48	0.59
(Gd/Yb)n	2.74	2.91	2.67	2.98	2.40	2.59	2.63	2.62	2.65	1.30	1.03	1.00
Eu/Eu*	1.02	0.91	1.05	1.00	0.98	0.99	0.99	1.00	1.03	1.00	1.02	0.96

calculations. Concordia diagrams and weighted mean calculations were made using Isoplot/Ex_ver3 [*Ludwig*, 2003]. Trace element compositions of zircons were calibrated against reference materials (BCR-2G and BIR-1G), combined with internal standardization [*Liu et al.*, 2010]. The preferred values of element concentrations for the USGS reference glasses were taken from the GeoReM database (http://georem.mpch-mainz.gwdg.de/).

5. Geochemical and Geochronological Results

5.1. Major and Trace Elements

The Yuejinshan and Raohe basalts from the Nadanhada Terrane have SiO_2 contents ranging from 45.67 to 51.70 wt %, total FeO from 10.46 to 13.74 wt%, MgO from 3.65 to 9.41 wt%, and TiO_2 from 1.21 to 3.39 wt% (Table 1). In the

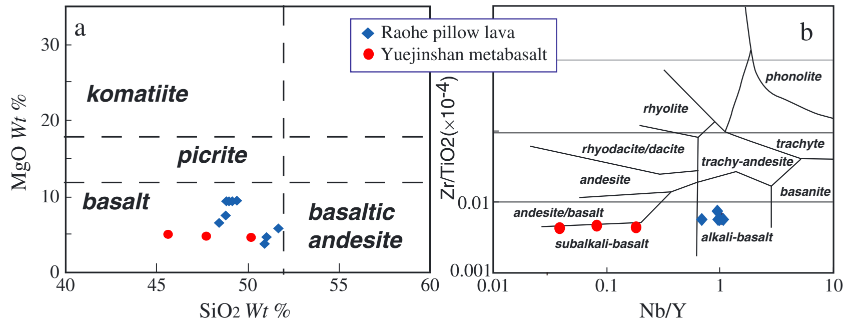

Figure 4. Geochemical classification of the Raohe pillow lavas and Yuejinshan metabasalts of the Nadanhada Terrane. (a) MgO versus SiO_2 diagram [after *Le Bas*, 2000]. (b) Zr/TiO_2 ($\times 10^{-4}$) versus Nb/Y diagram [after *Winchester and Floyd*, 1976].

MgO (wt%) vs. SiO_2 (wt%) diagram, all samples plot in the basalt field (Figure 4a). This signature is confirmed by the Zr/TiO_2 ($*10^{-4}$) vs. Nb/Y diagram (Figure 4b), which shows that all the Raohe basaltic pillow lavas plot in the alkali-basalt field, and the Yuejinshan metabasalts plot in the subalkali-basalt field, implying that they may be different in origin. The Nadanhada basaltic rocks can also be divided into two groups on the basis of their chondrite-normalized REE patterns (Figure 5a). Samples of the Yuejinshan metabasalt (04H-106, 108, and113) have somewhat lower ΣREE (53.2–69.87), lower LREE/HREE (2.47–2.79), and show weak LREE enrichment, with $(La/Yb)_N$ ratios ranging from 1.95 to 2.52. This pattern is characteristic of normal mid-ocean ridge basalt (N-MORB) (Figure 5a). In contrast, samples form the Raohe Complex (04H-70, 71,72,73, and 04H-80, 81,82,83,84) are strongly enriched in LREE (Figure 5a), with higher LREE/HREE (3.30–4.09) and $(La/Yb)_N$ ratios ranging from 5.13 to 8.12, similar to ocean island basalts (OIB) (Figure 5a). On a primitive mantle-normalized trace element variation diagram [*Sun and McDonough*, 1989] (Figure 5b), the Yuejinshan metabasalts have patterns similar to N-MORB, especially for the immobile elements (Ti, Zr, Y, and Nb). However, the contents of incompatible elements are elevated and show distinct spikes in Rb, Ba, Th, and U, possibly suggesting crustal contamination interaction during emplacement [*Pearce*, 2008]. The Raohe pillow lavas more closely approximate OIB but are relatively depleted in elements between Rb and U. All of the analyzed Nadanhada samples have relatively high Nb and Ta contents (Nb >1.73 ppm, Ta >0.14 ppm), distinguishing them from arc basalts. In the Ti/100-Zr-Y*3 and Nb*2-Zr/4-Y diagrams (Figures 6a and 6b), the Yuejinshan metabasalts plot in the MORB field, whereas the Raohe pillow lavas plot in the within-plate field. In the Zr/Yb vs. Zr diagram (Figure 7a), all the Raohe pillow lavas plot in the within-plate field and Yuejinshan metabasalts plot in the MORB field. In addition, on the Nb/Yb-Th/Yb diagram (Figure 7b), the Raohe pillow lavas plot close to OIB in the MORB-OIB array

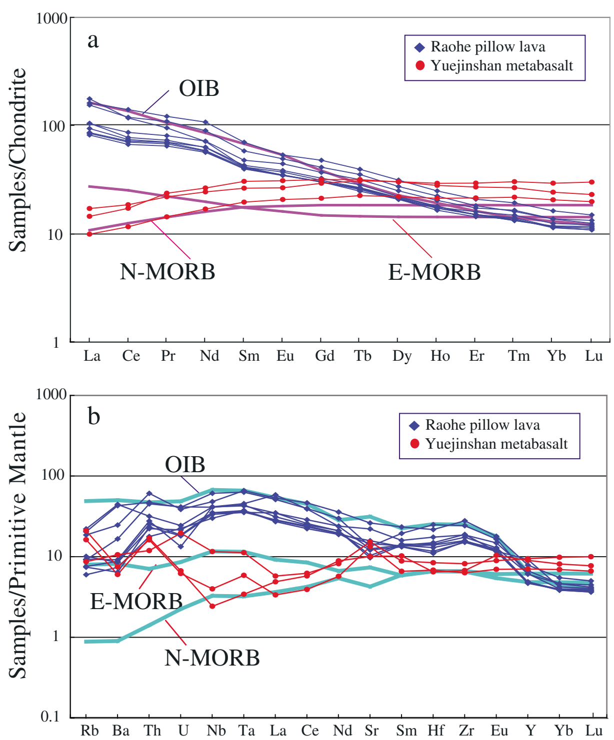

Figure 5. (a) Chondrite-normalized rare earth element (REE) diagram for the Raohe pillow lavas and Yuejinshan metabasalts of the Nadanhada Terrane [after *Sun and McDonough*, 1989]. (b) Primitive-mantle-normalized trace element diagram for the same rocks. The normalizing values for ocean island basalts (OIB), normal mid-ocean ridge basalt (N-MORB), and enriched mid-ocean ridge basalt (E-MORB) were taken from *Sun and McDonough* [1989] and *Stern* [2002].

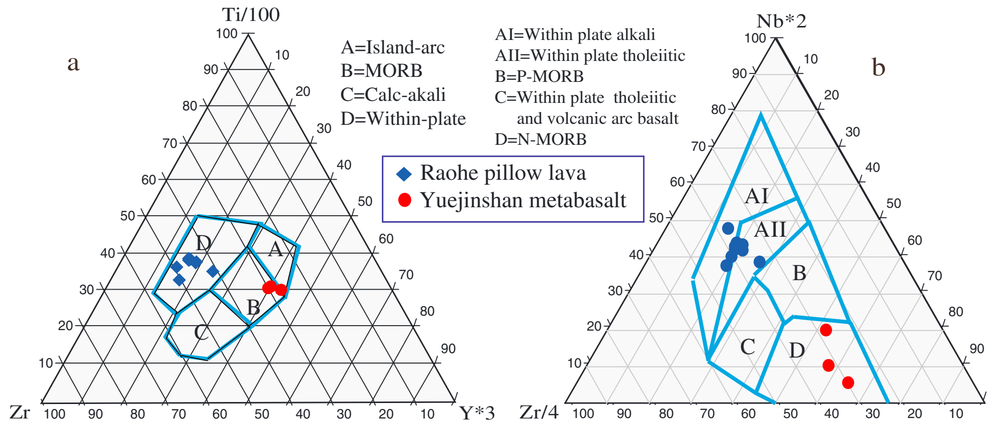

Figure 6. Basalt tectonic discrimination diagrams showing the compositions of both the Raohe pillow lavas and Yuejinshan metabasalts from the Nadanhada Terrane. (a) Ti/100-Zr-Y*3 plot (after *Pearce and Cann*, 1973). (b) Nb*3-Zr/4-Y plot (after *Meschede*, 1986).

whereas those from the Yuejinshan Complex plot above the MORB-OIB array, indicating the rocks possibly underwent crustal contamination [*Pearce*, 2008].

5.2. SHRIMP Zircon Ages

5.2.1. Gabbro (Sample RH-02) From the Raohe Complex

Zircons from sample RH-02 are colorless, transparent, and euhedral in shape. They range from ca. 150 to 200 μm in length, with length: width ratios of 3:1 to 4:1. CL imaging reveals that most grains are fairly dark with weak, banded zones (Figure 8a), characteristic of mafic rocks [*Koglin et al*., 2009; *Baines et al*., 2009; *Grimes et al*., 2009]. A total of 13 analyses were made on 13 zircons (Table 2), and they have U and Th contents and Th/U ratios ranging from 367 to 1674 ppm, 22 to 581 ppm, and 0.03 to 1.21 (most >0.2), respectively. The data are mostly concordant (Figure 8b), and four analyses (grains RH02-2, RH02-7, RH02-9, and RH02-10) define a weighted mean $^{206}Pb/^{238}U$ age of 216 ± 5 Ma (MSWD = 0.77), interpreted as the protolith age of the pillow lava. The other nine analyses yield apparent ages ranging from 231 ± 5 Ma to 440 ± 3 Ma. These old zircons are possibly inherited or xenocrystic, derived from the continental margin during magma emplacement.

5.2.2. Granite (Sample 04H-49)

Zircons from sample 04H-49 are colorless, transparent, and subhedral to euhedral in shape. They range from ca. 120 to 250 μm in length, with length: width ratios of 2:1 to 4:1. CL imaging reveals that most

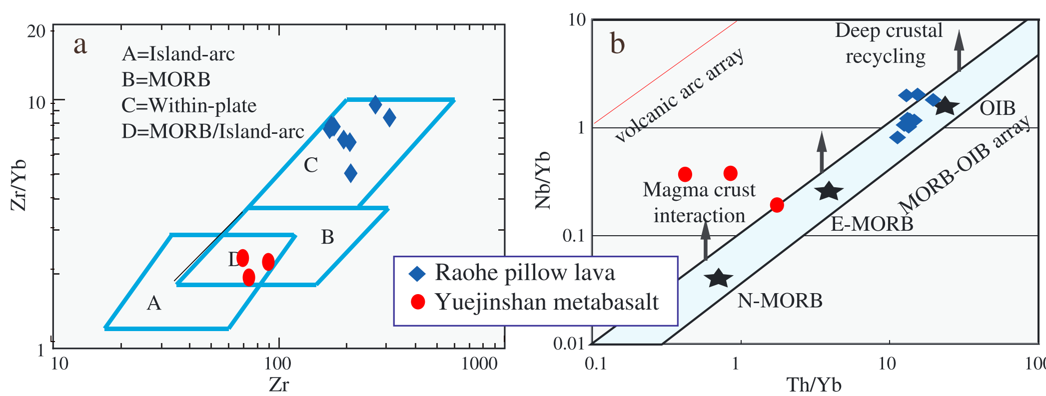

Figure 7. Basalt tectonic discrimination diagrams showing the compositions of the Raohe pillow lavas and Yuejinshan metabasalts from the Nadanhada Terrane. (a) Zr/Yb versus Zr plot [after *Pearce and Norry*, 1979] and (b) Nb/Yb versus Th/Yb plot [after *Pearce and Peate*, 1995].

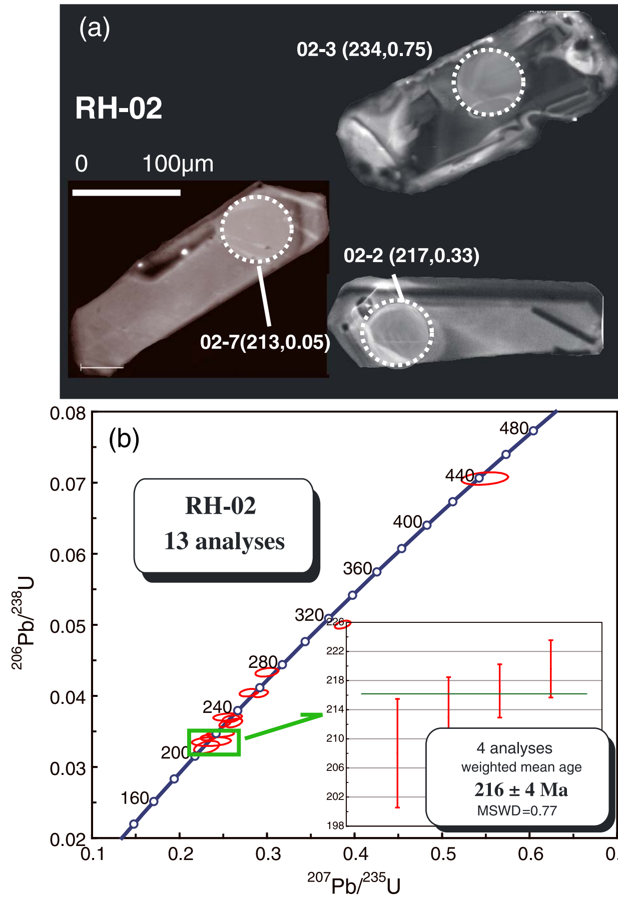

Figure 8. (a) Representative cathodoluminescence (CL) images of zircons from gabbro sample RH-02. Dotted circles mark sites of sensitive high-resolution ion microprobe (SHRIMP) analyses. The notation for each spot consists of spot number as in Table 2 and the age and Th/U ratio (in parentheses). (b) U-Pb concordia diagram of zircon data for gabbro sample RH-02 from the Raohe Complex.

grains have fine oscillatory zones (Figure 9a). A total of 12 analyses were made on 12 zircons (Table 2), and they have U and Th contents and Th/U ratios ranging from 277 to 708 ppm, 74 to 265 ppm, and 0.13 to 0.40, respectively. Eight of the analyses are concordant and define a weighted mean ^{206}Pb/^{238}U age of 128 ± 2 Ma (Figure 9b, MSWD = 1.9). Two other grains record ages of 135 ± 2 Ma (grain RH49-1, ^{206}Pb/^{238}U age) and 137 ± 2 Ma (grain RH49-3, ^{206}Pb/^{238}U age). In addition, one of the analyzed grains gives an older concordant age of 1890 ± 7 Ma (grain 49–4); these are inherited from unknown sources. The internal structures observed in CL and the Th/U ratios of the zircons suggest that the age of 128 ± 2 Ma is the formation age of the granite.

5.2.3. Granite (Sample 04H-69)

Zircons from sample 04H-69 are colorless, transparent, and subhedral to euhedral in shape. They range from ca. 120 to 200 μm in length, with length:width ratios of 2:1 to 3:1. CL imaging reveals that most grains have well-developed oscillatory zones (Figure 10a). A total of 13 analyses were made on 13 zircons (Table 2), and they have U and Th contents and Th/U ratios ranging from 123 to 921 ppm, 26 to 1237 ppm, and 0.12 to 1.39, respectively. The data are mostly concordant (Figure 10b) and 11 analyses define a weighted mean ^{206}Pb/^{238}U age of 129 ± 2 Ma (MSWD = 1.6). One grain yielded a discordant age of 170 ± 2 Ma (grain RH69-5, ^{206}Pb/^{238}U age). Another analyzed grain gives a younger age of 120 ± 2 Ma (grain RH69-7), possibly disturbed by a later intrusion. The uniformity in CL structure and generally moderate to high Th/U ratios (most >0.20, Table 2), indicate that the population at 129 ± 2 Ma defines the formation age of the granite.

5.3. LA-ICPMS Zircon Ages

5.3.1. Basaltic Pillow Lava (RH-08) From the Raohe Complex

Zircons from pillow lava sample RH-08 are colorless, transparent, and anhedral in shape (Figure 11a). They range in length from ca. 80 to 160 μm, with length:width ratios of 1:1 to 2:1. CL imaging reveals that all grains have weak banded zones (Figure 11a), indicative of a mafic-magmatic origin [*Koglin et al.*, 2009; *Baines et al.*, 2009; *Grimes et al.*, 2009]. A total of 30 analyses were made on 30 zircons (Table 3), and all analyses are concordant. The zircons have U and Th contents and Th/U ratios in the range of 186–6999 ppm, 67–17990 ppm, and 0.36–2.18, respectively, which is again consistent with a magmatic origin. Twenty-nine analyses define a weighted mean ^{206}Pb/^{238}U age of 167 ± 1 Ma (MSWD = 0.67; Figure 11b). One grain gave a ^{206}Pb/^{238}U ages of 178 ± 12 Ma (Table 3), and is interpreted to be inherited or xenocrystic. The banded zoning and Th/U ratios (most >0.4) of the zircons (Figure 11a and Table 3) indicate that the age of 167 ± 1 Ma represents the formation age of the pillow lava.

Table 2. Sensitive High-resolution Ion Microprobe (SHRIMP) Zircon U-Pb Data for Gabbro and Granite Samples From the Nadanhada Terrane[a]

Spot Number	U ppm	Th ppm	Th/U	$^{204}Pb/^{206}Pb$	$^{207}Pb^b/^{206}Pb^b$	±%	$^{207}Pb^b/^{235}U$	±%	$^{206}Pb^b/^{238}U$	±%	$^{206}Pb^b/^{238}U$ Age (Ma)		$^{207}Pb^b/^{206}Pb^b$ Age (Ma)	
Sample RH-02														
RH02-1	700	277	0.41	0.00006	0.0527	1.7	0.29	1.8	0.0403	0.8	255	2	315	19
RH02-2	919	290	0.33	0.00019	0.0495	2.4	0.23	2.6	0.0342	0.8	217	2	170	28
RH02-3	367	266	0.75	0.00017	0.0499	4.1	0.25	4.2	0.0370	0.9	234	2	192	48
RH02-4	1254	75	0.06	0.00005	0.0506	1.4	0.25	1.7	0.0361	0.9	229	2	224	17
RH02-5	1674	139	0.09	0.00026	0.0525	2.1	0.26	2.4	0.0362	1.1	229	3	308	24
RH02-6	536	581	1.12	0.00055	0.0564	3.1	0.55	3.2	0.0706	0.8	440	3	468	34
RH02-7	427	23	0.06	0.00112	0.0510	6.1	0.24	6.2	0.0336	1.2	213	3	243	70
RH02-8	473	125	0.27	0.00005	0.0501	2.4	0.28	2.6	0.0405	0.9	256	2	199	28
RH02-9	794	22	0.03	0.00046	0.0516	4.1	0.25	4.2	0.0347	0.8	220	2	268	47
RH02-10	694	150	0.22	0.00024	0.0511	3.7	0.23	4.1	0.0328	1.8	208	4	245	43
RH02-11	402	470	1.21	0.00004	0.0510	2.3	0.26	2.4	0.0368	0.9	233	2	242	26
RH02-12	1607	309	0.20	0.00016	0.0560	1.3	0.39	1.5	0.0500	0.7	315	2	453	15
RH02-13	923	317	0.36	0.00020	0.0502	2.7	0.30	2.9	0.0433	0.9	273	2	203	32
Sample RH-49														
RH49-1	596	77	0.13	0.00037	0.0511	2.4	0.13	4.9	0.0212	1.3	135	2	−22	57
RH49-2	548	198	0.37	0.00006	0.0481	2.7	0.13	3.5	0.0202	1.0	129	1	59	39
RH49-3	291	81	0.29	0.00015	0.0566	3.4	0.16	5.4	0.0215	1.2	137	2	388	59
RH49-4	708	86	0.13	0.00002	0.1159	0.8	5.51	1.4	0.3458	1.2	1914	19	1890	7
RH49-5	379	135	0.37	0.00116	0.0588	3.0	0.11	13.1	0.0194	1.3	124	2	−253	165
RH49-6	277	74	0.28	0.00044	0.0598	3.4	0.15	6.1	0.0201	1.3	128	2	348	67
RH49-7	365	86	0.24	0.00084	0.0567	4.0	0.12	10.6	0.0200	1.2	127	2	−98	130
RH49-8	531	204	0.40	0.00082	0.0531	2.7	0.12	9.2	0.0206	1.1	131	1	−297	117
RH49-9	313	89	0.29	0.00085	0.0557	3.3	0.12	10.0	0.0196	1.3	125	2	−161	123
RH49-10	528	188	0.37	0.00016	0.0535	2.5	0.14	4.8	0.0205	1.1	131	1	249	54
RH49-11	609	170	0.29	0.00052	0.0521	2.5	0.12	7.3	0.0204	1.1	130	1	−86	89
RH49-12	595	265	0.46	0.00039	0.0527	4.1	0.13	8.3	0.0204	1.1	130	1	43	99
Sample RH-69														
RH69-1	400	351	0.91	0.00034	0.0472	3.9	0.13	4.1	0.0196	1.3	125	2	58	93
RH69-2	266	31	0.12	0.00060	0.0604	8.0	0.16	8.2	0.0197	1.9	126	2	619	173
RH69-3	442	107	0.25	0.00025	0.0489	3.5	0.14	3.7	0.0203	1.3	130	2	145	82
RH69-4	711	158	0.23	0.00085	0.0469	5.6	0.13	5.8	0.0206	1.3	131	2	44	134
RH69-5	540	123	0.23	0.00007	0.0525	3.7	0.19	3.9	0.0268	1.2	170	2	309	85
RH69-6	387	251	0.67	0.00069	0.0486	6.8	0.13	7.1	0.0199	2.2	127	3	127	159
RH69-7	302	90	0.31	0.00040	0.0458	6.5	0.12	6.6	0.0188	1.3	120	2	−12	157
RH69-8	422	420	1.03	0.00056	0.0488	7.0	0.13	7.2	0.0199	1.4	127	2	139	165
RH69-9	123	62	0.52	0.00111	0.0458	14.4	0.13	14.5	0.0209	1.6	133	2	−12	348
RH69-10	376	299	0.82	0.00043	0.0493	4.8	0.14	5.0	0.0204	1.2	130	2	161	113
RH69-11	185	26	0.14	0.00020	0.0578	3.3	0.16	3.6	0.0201	1.3	128	2	521	73
RH69-12	921	1237	1.39	0.00018	0.0490	2.5	0.14	2.7	0.0204	1.1	130	1	149	59
RH69-13	261	45	0.18	0.00024	0.0460	4.1	0.12	4.3	0.0197	1.2	126	2	−3	99

[a]Errors are 1-sigma. Data were ^{204}Pb corrected, using measured values.
[b]indicates the radiogenic portions.

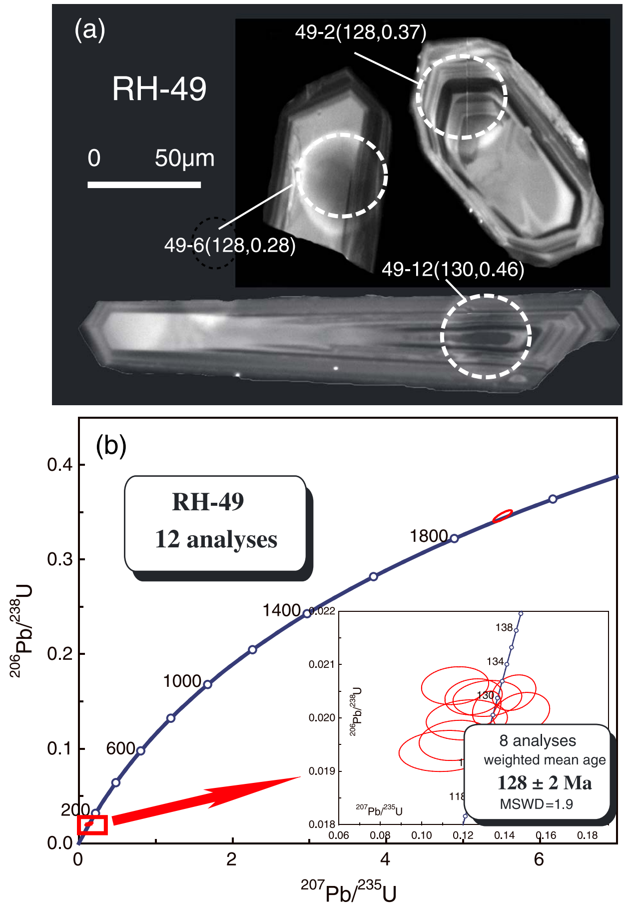

Figure 9. (a) Representative cathodoluminescence (CL) images of zircons from granite sample RH-49. Dashed circles mark sites of SHRIMP analyses. The notation for each spot is the same as in Figure 8. (b) U-Pb concordia diagram of zircon data for sample RH-49 from the Nadanhada Terrane.

5.3.2. Raohe Complex Sandstone (RH-05)

Zircons from sandstone sample RH-05 are small and subhedral, and range in size from 60 to 120 μm. CL imaging reveals that most grains show oscillatory zones (Figure 12a), indicative of a magmatic origin, although some have a core/rim structure. A total of 44 zircon analyses were obtained, and only four was discarded due to strong discordance. The zircons have U and Th contents and Th/U ratios in the range of 323–5652 ppm, 126–3936 ppm, and 0.15–1.20, respectively, which is suggestive of a magmatic origin. Amongst the 40 concordant analyses (Table 3), the grains yield apparent ages ranging from 2529 ± 28 to 136 ± 2 Ma (Figure 12b). In general, the results define three age populations according to their ^{206}Pb/^{238}U (<1000 Ma) or ^{207}Pb/^{2206}Pb ages (>1000 Ma). The age populations are at 136–182 Ma with a peak at 137 Ma, 348–569 Ma with a peak at 508 Ma, and 737–903 Ma with a peak at 785 Ma (Figure 12b), and one grain yields an older age of 2485 Ma. The four youngest grains define a weighted mean age of 137 ± 1 Ma (MSWD = 0.20; Figure 12b) and are interpreted to constrain the maximum depositional age of the sandstone.

5.3.3. Sandstone (RH-13) From the Raohe Complex

Sandstone sample RH-13 yielded abundant zircon grains, most of which are subhedral and range in size from 90 to 200 μm. CL imaging reveals that most grains have weak oscillatory zones (Figure 13a), indicative again of a magmatic origin. A total of 63 U-Pb analyses were obtained, and 10 analyses ware discarded due to strong discordance. The zircons have U and Th contents and Th/U ratios in the range of 97–3407 ppm, 72–2050 ppm, and 0.05–1.24, respectively, which is suggestive of a magmatic origin. Amongst the 53 concordant analyses (Table 3), the grains yield apparent ages ranging from 2415 ± 28 to 161 ± 4 Ma (Figure 13b). In general, the grains define five age populations: at 161–172 Ma with a peak at 167 Ma, 213–340 Ma with a peak at 263 Ma, 350–502 Ma with a peak at 463 Ma, 727–936 Ma with a peak at 745 Ma, and widely age population from 1765 to 2385 Ma (Figure 13b). The three youngest grains yield a weighted mean age of 167 ± 17 Ma (MSWD = 1.9) and are interpreted to constrain the maximum depositional age of the sandstone.

6. Discussion

6.1. Origin of the Mafic-Ultramafic Rocks From the Nadanhada Terrane

Triassic-Jurassic accretionary complexes are widely developed in NE China (Nadanhada), the Russian Far East (Sikhote-Alin), and SW Japan (e.g., Mino-Tanba; Figure 1). They may have constituted a continuous belt before the Miocene opening of the Japan Sea [*Mizutani et al.*, 1989; *Mizutani and Kojima*, 1992; *Kojima and Mizutani*, 1987; *Kojima*, 1989; *Zyabrev and Matsuoka*, 1999; *Zhang and Mizutani*, 2004]. However, the nature and origin of the complexes have long been disputed, with views ranging from ophiolitic sequences [*Mizutani et al.*, 1989; *Mizutani and Kojima*, 1992; *Cui*, 1986; *Kojima and Mizutani*, 1987; *Kojima*, 1989; *Kang et al.*, 1990; *Zhang*,

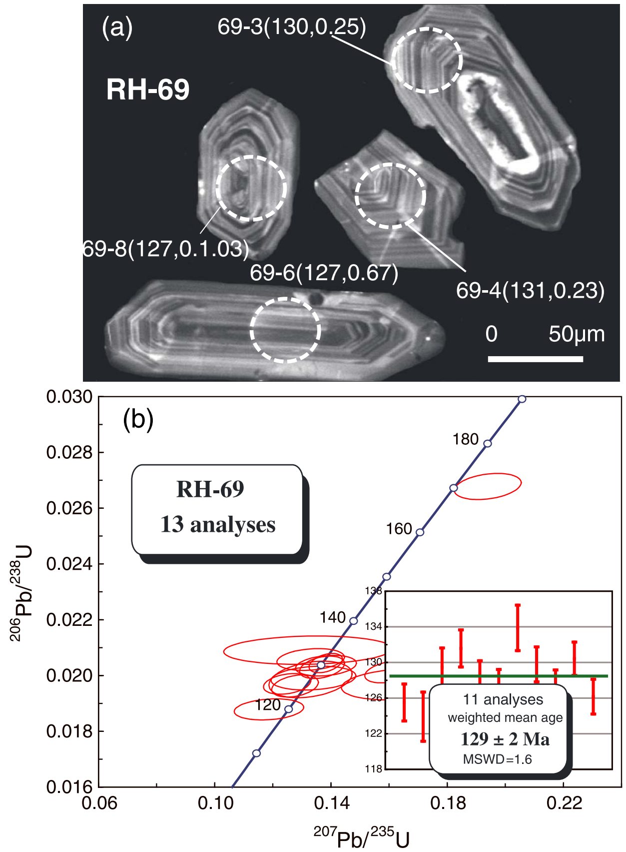

Figure 10. (a) Representative cathodoluminescence (CL) images of zircons from granite sample RH-69. Dashed circles mark sites of SHRIMP analyses. The notation for each spot is the same as in Figure 8. (b) U-Pb concordia diagram of zircon data for granite sample RH-69 from the Nadanhada Terrane.

1990; *Zhang and Mizutani*, 2004], ocean island sequences [*Zhang and Zhou*, 2001], or a superplume along a subduction zone [*Ishiwatari and Ichiyama*, 2004]. The mafic-ultramafic rocks therefore are the key to decipher the origin of the complex.

Our major, trace, and rare-earth element data for the Yuejinshan rocks show N-MORB affinity, whereas the Raohe pillow lavas have affinities to OIB (Figures 3–7). This is consistent with previous studies [*Zhang et al.*, 1997; *Zhang and Zhou*, 2001]. *Zhang et al.* [1997] reported that the Yuejinshan metabasalts at Hamadingzi (near Yuejinshan) have affinity to N-MORB. *Zhang and Zhou* [2001] pointed out that the Raohe mafic-ultramafic rocks most likely have OIB affinity. N-MORB characteristics are commonly formed at mid-ocean ridges or back-arc spreading centers [*Thompson et al.*, 1989; *Stern et al.*, 1995, 2002], whereas OIB features are normally considered to be associated with a plume source within an oceanic plate or a continental rift [*Doubleday et al.*, 1994]. The presence of both N-MORB and OIB in the same ophiolitic slices in the Flin Flon Belt in Canada [*Taira et al.*, 1992], western Tianshan [*Gao and Klemd*, 2003; *Klemd et al.*, 2011], northern Philippines [*Karig*, 1983], and Japan [*Taira*, 2001] has been interpreted to have of an intra-oceanic origin and were that the rocks amalgamated later in accretionary complexes.

Given that the pillow lavas and metabasalts of the Nadanhada Complex have OIB and N-MORB affinities, and they are associated with cumulate gabbro, radiolarian chert, and shale, it suggests that the complex was part of a subduction zone complex or ophiolitic mélange, similar to the Philippines intraoceanic accretionary complex formed by obduction of oceanic crust [*Stern et al.*, 1995; *Maruyama et al.*, 1997]. Therefore, the Nadanhada Complex is also an accretionary complex associated with paleo-Pacific subduction-accretion.

Early studies considered that that most mafic-ultramafic rocks in the Nadanhada Complex are Paleozoic in age, since they are covered by limestone and chert that contain Paleozoic to Mesozoic fossils. Some recent studies argued that some gabbros intruded into Triassic-Jurassic chert-shale-sandstone sequences, suggesting that the gabbro was Jurassic in age [*Cheng et al.*, 2006]. However, the mafic-ultramafic rocks only occur locally and are in tectonic contact with all other rock units (Figure 2b); thus, our new zircon U-Pb dating results provide important new evidence with respect to their age of formation.

SHRIMP data for the Raohe gabbro sample (RH-02) define a weighted mean age of 216 ± 5 Ma. The zircons have magmatic zoning and moderate Th/U ratios, indicating the age records the formation of the gabbro. These data (Table 2 and Figure 8), together with Late Triassic-Jurassic fossils from overlying bedded chert and siliceous shale obtained by *Kojima* [1989], indicate that the Raohe gabbro was formed at ~215 Ma, hence in the latest Triassic.

LA-ICPMS data from the Raohe basaltic pillow lava sample (RH-08) define a weighted mean age of 167 ± 1 Ma (Figure 11). The zircons have weak magmatic banding and moderate Th/U ratios, indicating that the age

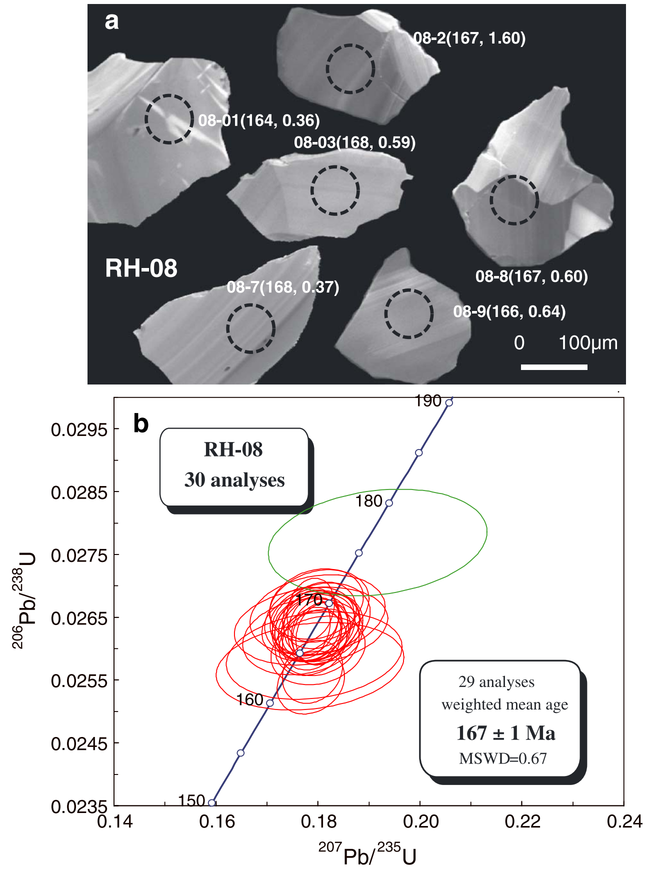

Figure 11. (a) Representative cathodoluminescence (CL) images of zircons from basaltic pillow lava sample RH-08. Dashed circles mark sites of laser ablation inductively coupled plasma mass spectrometry (LA-ICPMS) analyses. The notation for each spot is the same as in Figure 8. (b) U-Pb concordia diagram of zircon data for sample RH-08 from the Raohe Complex of the Nadanhada Terrane.

records the formation of the basaltic pillow lava. These new data are similar to the age from a nearby pillow lava, which yields a whole-rock Rb-Sr age of 169 ± 6 Ma [*Zhao et al.*, 1996] and an age of 168 ± 6 Ma by LA-ICPMS [*Cheng et al.*, 2006]. Therefore, the Raohe gabbro was formed in the latest Triassic (~215 Ma), whereas the Raohe basaltic pillow lava was formed in the Middle Jurassic (~170 Ma); thus, there is a range in the formation age for the mafic-ultramafic rocks from the latest Triassic to the Middle Jurassic (215–170 Ma).

6.2. Age of the Granite

SHRIMP data from the two granite samples (RH-49 and RH-69) define similar weighted mean ages of 128 ± 2 Ma and 129 ± 2 Ma (Figures 9 and 10), respectively. Zircons from both samples RH-49 and RH-69 have magmatic oscillatory zoning and moderate Th/U ratios, indicating that these ages record the formation of the granite. In addition, petrological studies indicate that the Raohe granite contains magmatic cordierite and has peraluminous characteristics, indicating its S-type affinity derived from partial melting of sedimentary rocks [*Cheng et al.*, 2006].

New data from our study, together with the LA-ICPMS magmatic zircon ages of 124 ± 1 Ma from a cordierite-bearing granite from the Hamahe pluton in the Raohe Complex obtained by *Cheng et al.* [2006], indicate the age of the granite is Early Cretaceous (~130 Ma).

6.3. Depositional Ages and Provenance of the Clastic Rocks

The clastic sample RH-13 from the Hongqiling area in the western part of the Raohe Complex yields a youngest concordant zircon age of 167 ± 17 Ma (Figure 13), whereas sample RH-05 from Dadai in the eastern part of the Raohe Complex contains abundant zircons with an age of 137 ± 3 Ma (Figure 12), suggesting a possible younging trend eastward toward the Pacific ocean.

The two clastic samples are important in providing additional constraints on the evolution of the Nadanhada Complex, since their detrital zircon populations have the potential to allow identification of sources no longer extant or possibly buried. They also provide a maximum age for deposition of the sedimentary protolith, which in this case is 137 ± 3 Ma. Sandstone sample RH-13 contains five main populations of near-concordant detrital zircon, with peak ages of ~167 Ma, 263 Ma, 463 Ma, and 745 Ma and a spread of ages between 1765 and 2385 Ma (Figure 13). In addition, siltstone sample RH-05 contains detrital zircon populations with peak ages of 137 Ma, 508 Ma, 785 Ma, and 2485 Ma (Figure 12). However, gabbro sample RH-02 contains inherited zircons with ages ranging from 240 Ma to 440 Ma. The age distributions partially match those recorded from the Mashan Complex from the Jiamusi Block analyzed by *Wilde et al.* [2000, 2003], and blueschists from the Jilin-Heilongjiang high-pressure metamorphic belt (Ji-Hei belt) analyzed by *Zhou et al.* [2009, 2013] and *Zhou and Wilde* [2013]. However, it should be noted that these rocks also contain

Table 3. Laser Ablation Inductively Coupled Plasma Mass Spectrometry (LA-ICPMS) Zircon U-Pb Data for Basalt and Sedimentary Samples From the Nadanhada Tarrane[a]

No.	Element (ppm)			Th/U	Isotope ratio						Apparent Age (Ma)						% Disc[c]
	Pb[b]	Th	U		^{207}Pb/^{206}U	1 s	^{207}Pb/^{235}U	1 s	^{206}Pb/^{238}U	1 s	^{207}Pb/^{206}Pb	1 s	^{207}Pb/^{235}U	1 s	^{207}Pb/^{238}U	1 s	
RH-05																	
RH-05-01	151	1098	1158	0.95	0.05175	0.00215	0.31	0.01	0.0432	0.0007	275	92	273	10	272	4	100
RH-05-02	153	1163	1163	1.00	0.05255	0.00383	0.30	0.02	0.0420	0.0009	310	157	270	17	265	5	98
RH-05-03	56	869	1122	0.78	0.04879	0.00285	0.14	0.01	0.0213	0.0004	138	132	136	7	136	2	100
RH-05-04	76	1327	877	1.51	0.04917	0.00398	0.15	0.01	0.0217	0.0005	156	179	139	10	138	3	99
RH-05-05	24	386	323	1.19	0.04887	0.00371	0.15	0.01	0.0229	0.0005	142	169	146	10	146	3	100
RH-05-06	59	935	815	1.15	0.04898	0.00349	0.14	0.01	0.0215	0.0004	147	159	137	9	137	3	100
RH-05-07	85	536	580	0.92	0.05348	0.00148	0.41	0.01	0.0554	0.0008	349	61	348	8	348	5	100
RH-05-08	413	2837	2592	1.09	0.06383	0.00120	0.37	0.01	0.0419	0.0006	736	39	318	5	264	3	83
RH-05-09	89	785	1668	0.47	0.04976	0.00144	0.20	0.01	0.0287	0.0004	184	66	183	5	182	2	100
RH-05-10	1498	7382	5458	1.35	0.05766	0.00077	0.65	0.01	0.0820	0.0010	517	29	510	6	508	6	100
RH-05-11	86	1124	935	1.20	0.04980	0.00308	0.19	0.01	0.0278	0.0005	186	138	177	10	177	3	100
RH-05-12	279	2826	3342	0.85	0.07124	0.00346	0.25	0.01	0.0254	0.0005	964	96	226	10	162	3	72
RH-05-13	162	944	1118	0.84	0.05351	0.00226	0.41	0.02	0.0550	0.0009	350	92	346	12	345	5	100
RH-05-14	313	415	1400	0.30	0.07559	0.00139	1.85	0.04	0.1776	0.0024	1084	37	1064	13	1054	13	99
RH-05-15	359	554	1536	0.36	0.05796	0.00334	0.69	0.04	0.0858	0.0016	528	122	530	23	531	9	100
RH-05-16	205	3936	2090	1.88	0.04931	0.00216	0.17	0.01	0.0248	0.0004	162	99	158	6	158	2	100
RH-05-17	37	328	1219	0.27	0.04879	0.00279	0.14	0.01	0.0213	0.0004	138	129	136	7	136	2	100
RH-05-18	62	433	2851	0.15	0.05682	0.00360	0.15	0.01	0.0190	0.0004	484	135	141	8	121	2	86
RH-05-19	126	955	1374	0.69	0.05410	0.00363	0.28	0.02	0.0372	0.0007	375	144	249	15	236	5	95
RH-05-20	591	435	646	0.67	0.16715	0.00276	10.76	0.19	0.4668	0.0065	2529	28	2503	16	2470	28	99
RH-05-21	269	773	2233	0.35	0.05759	0.00080	0.66	0.01	0.0830	0.0011	514	31	514	6	514	6	100
RH-05-22	133	1178	2851	0.41	0.06236	0.00146	0.23	0.01	0.0268	0.0004	686	49	211	5	171	2	81
RH-05-23	431	1493	5652	0.26	0.05659	0.00072	0.45	0.01	0.0578	0.0007	475	28	378	5	362	4	96
RH-05-24	85	487	1288	0.38	0.05370	0.00358	0.24	0.02	0.0326	0.0006	358	143	219	13	207	4	94
RH-05-25	132	668	801	0.83	0.05735	0.00136	0.64	0.02	0.0813	0.0012	504	52	504	10	504	7	100
RH-05-26	112	461	845	0.54	0.05779	0.00149	0.64	0.02	0.0805	0.0012	522	56	503	11	499	7	99
RH-05-27	81	270	544	0.50	0.06884	0.00131	1.43	0.03	0.1511	0.0021	894	39	903	12	907	12	100
RH-05-28	103	108	695	0.16	0.06468	0.00127	1.15	0.02	0.1285	0.0018	764	41	776	11	779	10	100
RH-05-29	282	2756	1547	1.78	0.06037	0.00177	0.69	0.02	0.0823	0.0012	617	62	530	12	510	7	96
RH-05-30	172	1376	1182	1.16	0.05975	0.00111	0.66	0.01	0.0802	0.0011	594	40	515	8	497	7	97
RH-05-31	118	167	753	0.22	0.06446	0.00096	1.15	0.02	0.1296	0.0018	757	31	778	9	785	10	101
RH-05-32	121	197	779	0.25	0.06604	0.00107	1.22	0.02	0.1337	0.0018	808	34	809	10	809	10	100
RH-05-33	101	351	729	0.48	0.06126	0.00154	0.89	0.02	0.1049	0.0015	648	53	645	12	643	9	100
RH-05-34	128	309	804	0.38	0.06453	0.00109	1.15	0.02	0.1291	0.0018	759	35	777	10	783	10	101
RH-05-35	112	230	649	0.35	0.06645	0.00118	1.22	0.02	0.1332	0.0018	821	37	810	11	806	10	99
RH-05-36	85	126	550	0.23	0.06516	0.00140	1.15	0.03	0.1283	0.0018	780	45	779	12	778	10	100
RH-05-37	147	633	1123	0.56	0.05756	0.00121	0.66	0.01	0.0826	0.0011	513	46	512	9	512	7	100
RH-05-38	74	252	585	0.43	0.05866	0.00295	0.74	0.04	0.0918	0.0016	555	106	564	21	566	10	100
RH-05-39	119	303	594	0.51	0.06629	0.00143	1.22	0.03	0.1338	0.0018	816	44	811	13	810	10	100
RH-05-40	194	433	1014	0.43	0.06631	0.00103	1.23	0.02	0.1343	0.0018	816	32	813	10	812	10	100
RH-05-41	454	961	3606	0.27	0.06421	0.00153	1.07	0.03	0.1213	0.0017	749	49	741	13	738	10	100
RH-05-42	567	834	4974	0.17	0.06408	0.00141	1.05	0.02	0.1193	0.0016	744	46	731	12	727	9	99
RH-05-43	53	418	1344	0.31	0.05260	0.00353	0.25	0.02	0.0350	0.0007	312	146	230	14	222	4	97
RH-05-44	463	839	2686	0.31	0.07025	0.00102	1.43	0.02	0.1479	0.0019	936	29	903	10	889	11	99
RH-08																	
RH-08-01	12	67	186	0.36	0.05032	0.00347	0.18	0.01	0.0257	0.0005	210	152	167	10	164	3	98
RH-08-02	616	5043	3153	1.60	0.04992	0.00100	0.18	0.00	0.0263	0.0003	191	46	169	3	167	2	99
RH-08-03	2092	17990	6999	2.57	0.04911	0.00069	0.18	0.00	0.0263	0.0003	153	32	167	2	168	2	101

Table 3. (continued)

No.	Element (ppm)			Th/U	Isotope ratio						Apparent Age (Ma)						% Disc[c]
	Pb[b]	Th	U		$^{207}Pb/^{206}U$	1 s	$^{207}Pb/^{235}U$	1 s	$^{206}Pb/^{238}U$	1 s	$^{207}Pb/^{206}Pb$	1 s	$^{207}Pb/^{235}U$	1 s	$^{207}Pb/^{238}U$	1 s	
RH-08-04	78	535	901	0.59	0.04950	0.00150	0.18	0.01	0.0264	0.0004	172	69	168	5	168	2	100
RH-08-05	59	442	636	0.69	0.04916	0.00175	0.18	0.01	0.0264	0.0004	156	81	167	5	168	2	100
RH-08-06	33	239	393	0.61	0.05021	0.00323	0.18	0.01	0.0259	0.0005	205	143	167	10	165	3	98
RH-08-07	16	95	255	0.37	0.04916	0.00275	0.18	0.01	0.0264	0.0004	156	126	167	9	168	3	100
RH-08-08	134	980	1626	0.60	0.04958	0.00102	0.18	0.00	0.0262	0.0003	175	47	167	3	167	2	100
RH-08-09	147	1103	1720	0.64	0.04966	0.00127	0.18	0.00	0.0261	0.0003	179	58	167	4	166	2	99
RH-08-10	149	1201	1260	0.95	0.04899	0.00176	0.18	0.01	0.0267	0.0004	148	82	168	6	170	2	101
RH-08-11	100	784	1000	0.78	0.05028	0.00170	0.18	0.01	0.0260	0.0004	208	77	168	5	165	2	98
RH-08-12	104	769	939	0.82	0.05008	0.00143	0.18	0.01	0.0261	0.0004	199	65	168	4	166	2	99
RH-08-13	208	1668	1757	0.95	0.05063	0.00107	0.18	0.00	0.0256	0.0003	224	48	167	3	163	2	98
RH-08-14	136	1018	1412	0.72	0.05087	0.00122	0.18	0.00	0.0255	0.0003	235	54	167	4	162	2	97
RH-08-15	62	446	694	0.64	0.04902	0.00217	0.18	0.01	0.0262	0.0004	149	101	166	7	167	3	101
RH-08-16	555	4764	2794	1.70	0.04959	0.00086	0.18	0.00	0.0263	0.0003	176	40	168	3	167	2	100
RH-08-17	110	844	1017	0.83	0.04932	0.00147	0.18	0.01	0.0263	0.0004	163	68	167	5	168	2	100
RH-08-18	796	6823	3777	1.81	0.04999	0.00089	0.18	0.00	0.0262	0.0003	194	41	169	3	167	2	99
RH-08-19	84	616	797	0.77	0.04945	0.00178	0.18	0.01	0.0265	0.0004	169	82	168	6	168	2	100
RH-08-20	880	7426	3403	2.18	0.04921	0.00128	0.18	0.00	0.0263	0.0004	158	60	167	4	168	2	100
RH-08-21	678	5916	2990	1.98	0.04865	0.00078	0.18	0.00	0.0266	0.0003	131	37	167	3	169	2	102
RH-08-22	91	711	733	0.97	0.04915	0.00145	0.18	0.01	0.0264	0.0004	155	67	167	5	168	2	100
RH-08-23	290	2472	1642	1.51	0.04905	0.00092	0.18	0.00	0.0264	0.0003	150	44	167	3	168	2	101
RH-08-24	209	1785	1374	1.30	0.04917	0.00109	0.18	0.00	0.0263	0.0003	156	51	167	4	167	2	100
RH-08-25	44	336	527	0.64	0.04918	0.00242	0.18	0.01	0.0265	0.0004	156	111	168	8	169	3	100
RH-08-26	72	544	727	0.75	0.04880	0.00164	0.18	0.01	0.0267	0.0004	138	77	168	5	170	2	101
RH-08-27	93	712	1027	0.69	0.04930	0.00128	0.18	0.00	0.0265	0.0004	162	60	168	4	169	2	100
RH-08-28	125	934	1402	0.67	0.04978	0.00144	0.18	0.01	0.0263	0.0004	185	66	169	5	168	2	99
RH-08-29	54	403	578	0.70	0.05021	0.00377	0.19	0.01	0.0277	0.0006	205	166	178	12	176	4	99
RH-08-30	73	568	816	0.70	0.04852	0.00130	0.18	0.00	0.0265	0.0004	125	62	165	4	168	2	102
RH-13																	
RH-13-01	22	72	110	0.65	0.05696	0.00181	0.58	0.02	0.0741	0.0011	489	69	466	12	461	6	99
RH-13-02	23	69	138	0.50	0.06941	0.00100	1.50	0.02	0.1563	0.0020	911	29	929	10	936	11	101
RH-13-03	420	340	534	0.64	0.05125	0.00112	0.29	0.01	0.0404	0.0005	252	49	255	5	255	3	100
RH-13-04	410	189	189	1.00	0.04923	0.00217	0.18	0.01	0.0264	0.0004	159	100	167	7	168	3	100
RH-13-05	404	372	594	0.63	0.05064	0.00081	0.28	0.00	0.0406	0.0005	225	37	254	4	257	3	101
RH-13-06	80	597	406	1.47	0.05097	0.00098	0.26	0.01	0.0366	0.0005	240	44	233	4	232	3	100
RH-13-07	153	700	2187	0.32	0.05265	0.00106	0.32	0.01	0.0437	0.0006	314	45	280	5	276	4	99
RH-13-08	1195	1017	1345	0.76	0.11574	0.00152	5.31	0.08	0.3325	0.0043	1892	23	1870	13	1851	21	99
RH-13-09	169	878	2348	0.37	0.05107	0.00117	0.28	0.01	0.0391	0.0005	244	52	247	5	247	3	100
RH-13-10	76	103	236	0.44	0.07005	0.00396	1.45	0.08	0.1503	0.0030	930	112	911	33	903	17	99
RH-13-11	88	75	361	0.21	0.11508	0.00401	2.55	0.09	0.1606	0.0027	1881	61	1286	25	960	15	75
RH-13-12	80	271	606	0.45	0.05471	0.00653	0.45	0.05	0.0602	0.0018	400	248	380	37	377	11	99
RH-13-13	75	518	697	0.74	0.05050	0.00785	0.24	0.04	0.0349	0.0013	218	325	221	30	221	8	100
RH-13-14	489	118	2269	0.05	0.09815	0.00279	3.24	0.09	0.2395	0.0037	1589	52	1467	22	1384	19	94
RH-13-15	75	384	641	0.60	0.05700	0.00453	0.29	0.02	0.0370	0.0008	491	167	259	18	234	5	90
RH-13-16	626	535	681	0.79	0.16052	0.00183	6.80	0.09	0.3073	0.0039	2461	19	2086	12	1727	19	83
RH-13-17	413	283	656	0.43	0.13600	0.00325	7.03	0.17	0.3749	0.0057	2177	41	2115	21	2053	27	97
RH-13-18	157	805	1208	0.67	0.05490	0.00444	0.32	0.02	0.0417	0.0009	408	171	278	19	263	6	95
RH-13-19	1634	1482	2931	0.51	0.12020	0.00269	5.82	0.13	0.3513	0.0051	1959	39	1950	20	1941	25	100
RH-13-20	1281	518	3363	0.15	0.10407	0.00135	3.09	0.05	0.2156	0.0028	1698	24	1431	11	1258	15	88
RH-13-21	563	1875	3059	0.61	0.05831	0.00187	0.60	0.02	0.0746	0.0011	541	69	477	12	464	7	97

Table 3. (continued)

	Element (ppm)				Isotope ratio						Apparent Age (Ma)						
No.	Pb[b]	Th	U	Th/U	$^{207}Pb/^{206}U$	1 s	$^{207}Pb/^{235}U$	1 s	$^{206}Pb/^{238}U$	1 s	$^{207}Pb/^{206}Pb$	1 s	$^{207}Pb/^{235}U$	1 s	$^{207}Pb/^{238}U$	1 s	% Disc[c]
RH-13-22	44	309	426	0.72	0.05241	0.00588	0.24	0.03	0.0336	0.0009	303	237	221	22	213	6	97
RH-13-23	693	768	1188	0.65	0.16017	0.00257	9.29	0.16	0.4208	0.0058	2457	27	2367	16	2264	26	96
RH-13-24	114	420	558	0.75	0.05660	0.00447	0.45	0.03	0.0573	0.0013	475	166	375	24	359	8	96
RH-13-25	1022	759	1922	0.39	0.10830	0.00220	4.63	0.10	0.3101	0.0044	1771	37	1755	18	1741	21	99
RH-13-26	142	180	1447	0.12	0.06201	0.00269	0.64	0.03	0.0745	0.0012	674	90	501	17	464	7	93
RH-13-27	102	205	272	0.76	0.06553	0.00564	1.08	0.09	0.1195	0.0031	791	171	743	44	727	18	98
RH-13-28	474	101	1577	0.06	0.10916	0.00450	4.76	0.19	0.3164	0.0059	1786	73	1778	34	1772	29	100
RH-13-29	167	1212	1593	0.76	0.05242	0.00327	0.30	0.02	0.0414	0.0008	304	136	266	14	261	5	98
RH-13-30	1011	623	1229	0.51	0.15826	0.00245	8.68	0.15	0.3979	0.0054	2437	26	2305	15	2160	25	94
RH-13-31	137	863	933	0.93	0.05113	0.00614	0.30	0.03	0.0421	0.0013	247	255	264	27	266	8	101
RH-13-32	524	240	1536	0.16	0.11475	0.00189	4.82	0.09	0.3048	0.0041	1876	29	1789	15	1715	20	96
RH-13-33	2373	1705	2991	0.57	0.15404	0.00165	9.49	0.12	0.4471	0.0057	2391	18	2387	12	2382	25	100
RH-13-34	299	2050	2503	0.82	0.06489	0.00388	0.45	0.03	0.0504	0.0010	771	121	378	18	317	6	84
RH-13-35	148	627	1612	0.39	0.05621	0.00289	0.29	0.01	0.0374	0.0007	460	111	258	12	237	4	92
RH-13-36	152	772	1863	0.41	0.05154	0.00146	0.28	0.01	0.0397	0.0006	265	64	253	6	251	3	99
RH-13-37	561	914	1086	0.84	0.09293	0.00238	2.90	0.08	0.2261	0.0033	1486	48	1381	20	1314	17	95
RH-13-38	187	627	1300	0.48	0.05973	0.00527	0.39	0.03	0.0477	0.0012	594	181	336	25	300	7	89
RH-13-39	233	1016	3407	0.30	0.05212	0.00106	0.30	0.01	0.0421	0.0006	291	46	268	5	266	3	99
RH-13-40	82	361	420	0.86	0.05084	0.00699	0.30	0.04	0.0435	0.0014	234	290	270	32	274	9	102
RH-13-41	152	129	243	0.53	0.12532	0.00453	6.26	0.22	0.3626	0.0066	2033	63	2014	31	1995	31	99
RH-13-42	125	599	1075	0.56	0.05365	0.00334	0.26	0.02	0.0356	0.0007	356	134	237	13	225	4	95
RH-13-43	199	866	1875	0.46	0.06101	0.00175	0.45	0.01	0.0536	0.0008	640	60	378	9	336	5	89
RH-13-44	82	407	638	0.64	0.05149	0.00593	0.27	0.03	0.0378	0.0011	263	245	242	24	239	7	99
RH-13-45	304	116	1076	0.11	0.11283	0.00323	4.98	0.14	0.3201	0.0051	1846	51	1816	24	1790	25	99
RH-13-46	25	72	97	0.74	0.08410	0.02248	0.55	0.14	0.0477	0.0034	1295	447	447	93	300	21	67
RH-13-47	418	347	899	0.39	0.07383	0.00276	1.24	0.05	0.1220	0.0020	1037	74	820	21	742	11	91
RH-13-48	115	556	951	0.58	0.05274	0.00318	0.28	0.02	0.0385	0.0007	318	131	251	13	244	4	97
RH-13-49	680	577	705	0.82	0.11885	0.00130	5.71	0.08	0.3487	0.0044	1939	19	1933	11	1929	21	100
RH-13-50	126	723	938	0.77	0.05162	0.00159	0.30	0.01	0.0417	0.0006	268	69	264	7	263	4	100
RH-13-51	1267	787	1519	0.52	0.15621	0.00263	9.56	0.17	0.4440	0.0062	2415	28	2393	17	2369	27	99
RH-13-52	159	784	708	1.11	0.05388	0.00313	0.44	0.02	0.0586	0.0011	366	126	367	18	367	6	100
RH-13-53	290	1797	3012	0.60	0.05230	0.00259	0.30	0.01	0.0417	0.0007	299	109	267	11	264	4	99
RH-13-54	240	760	1372	0.55	0.05895	0.00133	0.66	0.02	0.0810	0.0011	565	49	513	9	502	7	98
RH-13-55	302	265	443	0.60	0.11096	0.00473	4.78	0.20	0.3128	0.0060	1815	75	1782	35	1754	30	98
RH-13-56	95	836	676	1.24	0.05125	0.00692	0.19	0.03	0.0271	0.0009	252	283	178	22	172	5	97
RH-13-57	176	757	996	0.76	0.05209	0.00444	0.40	0.03	0.0556	0.0013	290	183	341	24	349	8	102
RH-13-58	89	736	1093	0.67	0.05294	0.00468	0.18	0.02	0.0252	0.0006	326	189	172	14	161	4	94
RH-13-59	136	1012	891	1.14	0.05167	0.00122	0.28	0.01	0.0392	0.0005	271	53	250	5	248	3	99
RH-13-60	1904	1212	1973	0.61	0.14850	0.00188	8.80	0.13	0.4297	0.0056	2329	22	2317	13	2304	25	99

[a]Errors are 1-sigma.
[b]Indicates the corrected radiogenic portions.
[c]Disc = % discordance defined as $[(^{206}Pb/^{238}age)/(^{207}Pb/^{235}U)] \times 100$.

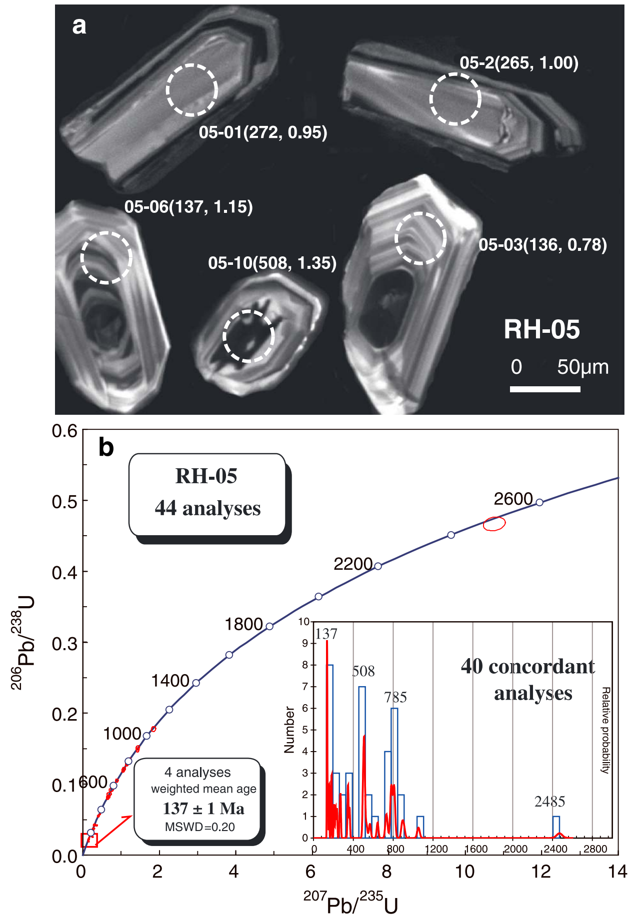

Figure 12. (a) Representative cathodoluminescence (CL) images of detrital zircons from siltstone sample RH-05. Dashed circles mark sites of LA-ICPMS analyses. The notation for each spot is the same as in Figure 8. (b) U-Pb concordia diagram of detrital zircon data for sample RH-05 from the Raohe Complex of the Nadanhada Terrane.

populations at 910–670 Ma, as well as two older grains with ages of 1065 and 2140 Ma. These detrital and the inherited zircons establish the presence of Pan-African and Neoproterozoic source material in the area. In the case of the inherited zircons in the gabbro, these were likely present in the basement when the mafic magma was emplaced. The detrital zircons in the clastic rocks may potentially have been derived in part from outside of the current Jiamusi Block. Therefore, we suggest that the clastic rocks were the trench-fill terrigenous rocks along the continental slope adjacent to the Jiamusi-Khanka Block.

6.4. Timing of Emplacement of the Nadanhada Accretionary Complex

The Nadanhada accretionary complex has been recognized as a mélange that contains tectonic lenses of limestone, greenstone (mafic-ultramafic sequences), bedded chert and siliceous shale, and clastic sediments, all intruded by granite [*Mizutani et al.*, 1989; *Kojima and Mizutani*, 1987; *Kojima*, 1989; *Cheng et al.*, 2006]. Available radiolarian and geological evidence limit the timing of emplacement of the Nadanhada Complex to the Late Jurassic-Early Cretaceous [*Kojima*, 1989; *Cheng et al.*, 2006].

In addition, gabbro sample RH-02 from Guanmen in the Raohe Complex formed at 216 ± 4 Ma (Figure 8), whereas pillow lava from Dadai formed at 167 ± 1 Ma (Figure 11), indicating that the mafic-ultramafic sequences of the Raohe Complex formed during the Late Triassic to Middle Jurassic. Sandstone sample RH-13 from Hongqiling in the western part of the Raohe Complex records detrital zircon U-Pb ages ranging from 2415 ± 28 to 161 ± 4 Ma (Figure 13), with the youngest age populations at 172–161 Ma and a peak at 167 Ma, whereas siltstone sample RH-05 from the eastern part of the Raohe Complex yields detrital zircon U-Pb ages ranging from 2529 ± 28 to 136 ± 2 Ma (Figure 12), with the youngest age population of 136–182 Ma with a peak age at 137 Ma. These data indicate that the deposition age of the clastic rocks should be around 167 and 136 Ma, with an eastward younging trend toward the Pacific Ocean. These data, together with the fossil evidence from limestone, indicate that the main part of the Raohe Complex consists of Carboniferous to Permian limestone, Late Triassic-Middle Jurassic mafic-ultramafic sequences, Triassic-Middle Jurassic bedded chert and siliceous shale, and Late Jurassic-Early Cretaceous clastic rocks.

New high-quality zircon U-Pb data from this study indicate that both granite samples formed at ~128 Ma (Figures 9 and 10). This means that the sedimentary rocks were lithified and deformed prior to the granite emplacement, and this must have occurred in the short time interval between the 136 and 128 Ma.

7. Tectonic Implications

The Nadanhada Terrane is composed of the Raohe and Yuejinshan complexes. *Kojima* [1989] noted that prior to opening of the Sea of Japan, the Japanese Islands were located much closer to the eastern margin of the

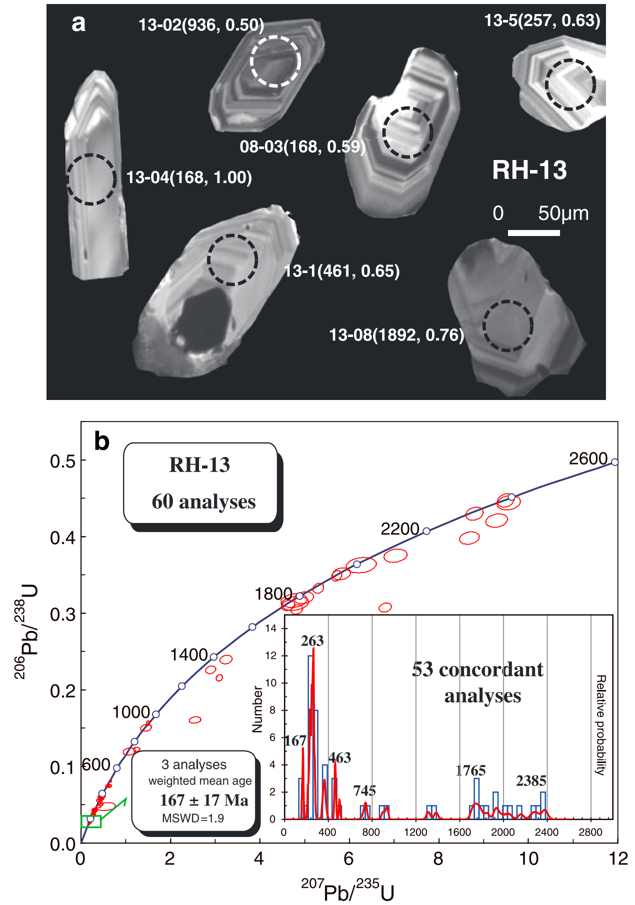

Figure 13. (a) Representative cathodoluminescence (CL) images of detrital zircons from sandstone sample RH-13. Dashed circles mark sites of LA-ICPMS analyses. The notation for each spot is the same as in Figure 8. (b) U-Pb concordia diagram of detrital zircon data for sample RH-13 from the Raohe Complex of the Nadanhada Terrane.

Asian continent where the Nadanhada and Sikhote-Alin terranes are now exposed. The Mino-Tamba Terrane in central Japan has the same characteristics of these terranes [*Kojima*, 1989; *Zhang and Mizutani*, 2004; *Zyabrev and Matsuoka*, 1999]. The paleobiological data, together with the geochronological data from this study, indicate that the accretion of the Raohe Complex to the CAOB occurred between the Late Jurassic and Early Cretaceous (170–136 Ma), and was completed by the Early Cretaceous (130 Ma). Unfortunately, insufficient zircons were available for analyses from the Yuejinshan N-MORB metabasalts to enable us to date these rocks. The information available for the Yuejinshan Complex indicates that it has undergone greenschist-facies metamorphism with a deformation at 188 ± 3 Ma [*Yang et al.*, 1998]. In addition, high-pressure metamorphic blueschist is widely exposed in the Jilin-Heilongjiang high-pressure metamorphic belt (Ji-Hei belt) along the western margin of the Jiamusi-Khanka Block [*Zhou et al.*, 2009, 2013; *Zhou and Wilde*, 2013; Figures 1 and 2a]. Magmatic zircons extracted from two samples of epidote-blueschist facies metabasalts from Mudanjiang of the Ji-Hei belt have SHRIMP U-Pb $^{206}Pb/^{238}U$ ages of 213 ± 2 Ma and 224 ± 7 Ma [*Zhou et al.*, 2009], whereas the biotite Rb-Sr mineral isochron age of 184 ± 4 Ma from a dioritic gneiss from Luobei, and three samples of mica schist from Yilan gave phengite $^{40}Ar/^{39Ar}$ ages of 173.6 ± 0.5 Ma, 175.3 ± 0.4 Ma and 174.8 ± 0.5 Ma [*Wu et al.*, 2007]. These data indicated that the metamorphism of the Ji-Hei belt took place between 210 and 180 Ma, and was related to the onset of paleo-Pacific plate subduction [*Zhou et al.*, 2009, 2010a, 2013; *Zhou and Wilde*, 2013]. Furthermore, Late Triassic granitics (223–212 Ma) with active continental margin setiting also occur in the Khanka area along the western margin of the Nadanhada Terrane [*Hao et al.*, 2014]. This further suggests that paleo-Pacific plate subduction was westward-directed at this time, and that the Yuejinshan Complex probably formed between 210 and 180 Ma. Based on our new data, the tectonic model for the paleo-Pacific plate subduction-accretion of the Nadanhada accretionary complex is as follows.

Late Triassic to Early Jurassic (210–180 Ma) is the time when a switch in geodynamic setting occurred between southward closure of the CAOB and the onset of westward-directed accretion related to Pacific plate subduction [*Zhou et al.*, 2009, 2013; *Zhou and Wilde*, 2013]. Westward obduction of the paleo-Pacific plate over the Jiamusi-Khanka Block resulted in the emplacement of the Yuejinshan Complex. At the same time, the Heilongjiang high-pressure metamorphic belt was formed, also as a result of paleo-Pacific subduction (Figure 14a).

During the Early Jurassic-Early Cretaceous (180–130 Ma). The Pacific oceanic plate with Early Jurassic seamounts collided with the CAOB continental margin and brought associated limestone, bedded chert, and siliceous shale. Enormous amounts of clastic detritus started filling the trench and continental slope. Tectonic

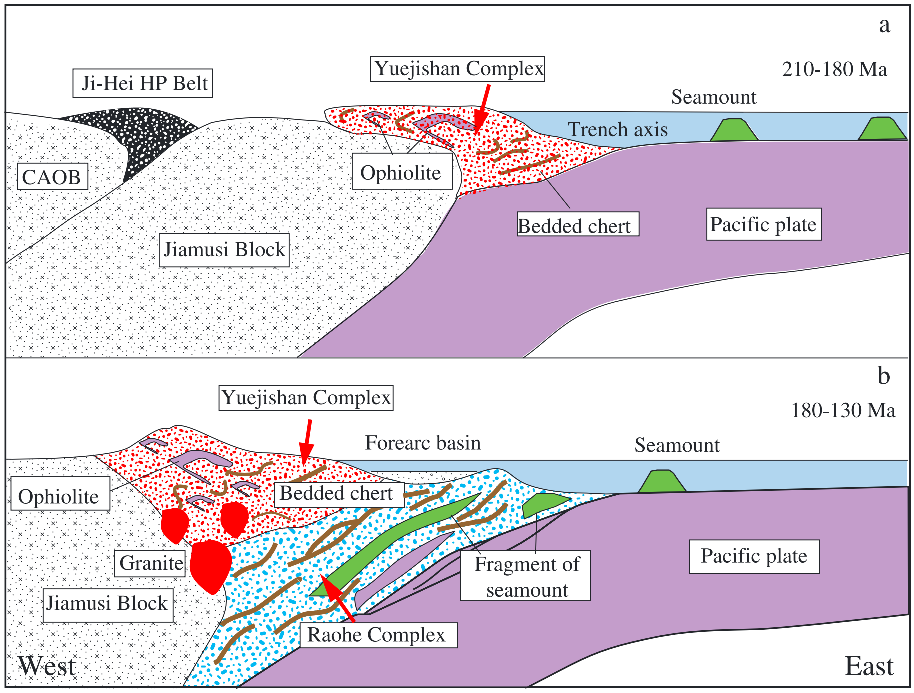

Figure 14. A cartoon sketches of the proposed tectonic setting of the Nadanhada Terrane resulting from Paleo-Pacific subduction-accretion between (a) 210–180 Ma and (b) 180–130 Ma.

activity resulted in jumbling and telescoping of pelagic sediments in the accretionary complex between 180 and 137 Ma. The final emplacement of the Nadanhada Terrane was at 137–130 Ma, and it was then intruded by the Early Cretaceous S-type granites (Figure 14b).

8. Conclusions

The Nadanhada Terrane is composed of the Yuejinshan and Raohe complexes. The Yuejinshan Complex is located closest to the CAOB and consists of both meta-clastic rocks and metamafic-ultramafic rocks that experienced lower greenschist-facies metamorphism. The Raohe Complex consists of limestone, bedded chert, siliceous claystone, and mafic-ultramafic rocks that are embedded as olistoliths in a weakly sheared clastic matrix.

Metabasalts in the Yuejinshan Complex have N-MORB affinity, whereas the basalts in the Raohe Complex have affinity to OIB. Given that the basaltic rocks of the Nadanhada Terrane have both OIB and N-MORB affinities, and are associated with cumulate gabbro, radiolarian chert, and shale, the Nadanhada Complex is interpreted as part of a subduction complex.

SHRIMP U-Pb zircon analyses of gabbro associated with the Raohe Complex yield a weighted mean ^{206}Pb/^{238}U zircon age of 216 ± 5 Ma, and two samples of granite intruded into the complex yield weighted mean ^{206}Pb/^{238}U zircon ages of ~128 Ma. LA-ICPMS U-Pb zircon analyses of basaltic pillow lava from the Raohe Complex record a weighted mean age of 167 ± 1 Ma, defining the formation age of mafic volcanic rocks of the Raohe Complex. In addition, a sandstone sample from Hongiling records detrital zircon ages ranging from 2415 ± 28 to 161 ± 4 Ma, with the youngest concordant zircons defining a weighted mean age of 167 ± 17 Ma. However, another sandstone sample from Dadai contains detrital zircon ages ranging from 2529 ± 28 to 136 ± 2 Ma, and the youngest concordant zircons define a weighted mean age of 137 ± 3 Ma. These constrain the maximum time of deposition and show a younging trend toward the Pacific Ocean in the east. Both sandstone samples contain abundant detrital zircons with peak ages of ~500 Ma and 700–900 Ma, similar to the age populations of rocks in the Jiamusi-Khanka Block, suggesting they are trench-fill terrigenous clastic rocks formed along the continental slope adjacent to the Jiamusi-Khanka Block.

The formation age of the Raohe Complex was from the Late Jurassic to Early-Cretaceous (170–137 Ma), and final accretion took place in the Early Cretaceous (137–130 Ma). The Yuejinshan Complex probably formed between 210 and 180 Ma, although no precise data are available. It is likely of similar age to the Jilin-Heilongjiang high-pressure metamorphic belt (Ji-Hei belt) along the western margin of the Jiamusi-Khanka Block, where the Heilongjiang blueschists formed between 210 and 180 Ma. Both the Ji-Hei belt on the western margin of the Jiamusi-Khanka Block and the Nadanhada Terrane on its eastern margin are the products of paleo-Pacific subduction.

Acknowledgments
This work was funded by grants from the Natural Science Foundation of China (41390441, 41190075, and 41272241), the Ministry of Science and Technology of China (2013CB429802), and the Chinese Geological Survey (1212011120153). The final version of this paper benefited from the perceptive comments by Nathan Niemi (Editor), Wen-Jiao Xiao, and Min Sun. This work is a contribution to the IGCP 592.

References

Andersen, T. (2003), Correction of common lead in U–Pb analyses that do not report ^{204}Pb, *Chem. Geol.*, *192*, 59–79.
Baines, A. G., M. J. Cheadle, B. E. John, C. B. Grimes, J. J. Schwartz, and J. L. Wooden (2009), SHRIMP Pb/U zircon ages constrain gabbroic crustal accretion at Atlantis Bank on the ultraslow-spreading Southwest Indian Ridge, *Earth Planet. Sci. Lett.*, *287*, 540–550.
Cheng, R. Y., F.,. Y. Wu, W. C. Ge, D. Y. Sun, X. M. Liu, and J. H. Yang (2006), Emplacement age of the Raohe Complex in eastern Heilongjiang Province and the Tectonic evolution of the eastern part of Northeastern China [in Chinese with English abstract], *Acta Petrol. Sin.*, *22*, 353–376.
Compston, W., I. S. Williams, and C. Meyer (1984), U–Pb geochronology of zircons from Lunar breccia 73217 using a sensitive high mass-resolution ion microprobe, *J. Geophys. Res.*, *89*, 525–534, doi:10.1029/JB089iS02p0B525.
Cui, X. S. (1986), A discovery of spinifex of komatiite in Mesozoic plate subduectied zone in Nadanhada Range, Heilongjiang Province. Contributions for the Project of Plate Tectonics in Northern China (1). Beijing: [in Chinese with English abstract], *Geol. Pub. House*, *199–207*.
Ding, Q. H., Q. Y. Zhang, and Y. H. Gao (1997), Research on Middle-Triassic to Middle Jurassic stratigraphy on Nadanhada Rannge, Memoirs of Shenyang Institute of Geology and Mineral Resources [in Chinese with English abstract], *Chin. Acad. Geol. Sci.*, *5–6*, 269–285.
Doubleday, R. A., P. T. Leat, T. Alabaster, P. A. R. Nell, and T. H. Tranter (1994), Allochthonous oceanic basalts within the Mesozoic accretionary complex of Alexander Island, Antarctic: Remnants of proto-Pacific oceanic crust, *J. Geol. Soc. London*, *151*, 65–78.
Faure, M., and B. Natal'in (1992), The geodynamic evolution of the eastern Eurasian margin in Mesozoic times, *Tectonophysics*, *208*, 397–411.
Gao, J., and R. Klemd (2003), Formation of HP–LT rocks and their tectonic implications in the western Tianshan Orogen, NW China: Geochemical and age constraints, *Lithos*, *66*, 1–22.
Grimes, C. B., B. E. John, M. J. Cheadle, F. K. Mazdab, J. L. Wooden, S. Swapp, and J. J. Schwartz (2009), On the occurrence, trace element geochemistry, and crystallization history of zircon from in situ ocean lithosphere. Contrib, *Mineral. Petrol.*, *158*, 757–783.
Hao, Y., W. C. Ge, G. C. Zhao, J. J. Yu, and Y. L. Zhang (2014), Early Permian–Late Triassic granitic magmatismin the Jiamusi–Khanka Massif, eastern segment of the Central Asian Orogenic Belt and its implications, *Gondwana Res.*, doi:10.1016/j.gr.2014.01.011.
Heilongjiang Bureau of Geology and Mineral Resources (HBGMR) (1987), 1:200000 Regional geological Map of Xaojiahe and Raohe Beijing: [in Chinese], *Geol. Publ. House*.
Heilongjiang Bureau of Geology and Mineral Resources (HBGMR) (1993), Regional geology of Heilongjiang Province. Beijing: [in Chinese with English abstract], *Geol. Publ. House*, 347–418.
Hu, Z. C., S. Gao, Y. S. Liu, S. H. Hu, H. H. Chen, and H. L. Yuan (2008), Signal enhancement in laser ablation ICP-MS by addition of nitrogen in the central channel gas, *J. Anal. At. Spectrom.*, *23*, 1093–1101.
Ishiwatari, A., and Y. Ichiyama (2004), Alaskan-type plutons and ultramafic lavas in Far East Russia, Northeast China, and Japan, *Int. Geol. Rev.*, *46*, 316–331.
Kang, B. X., H. R. Zhang, C. S. Liu, X. S. Cui, and S. F. Zhang (1990), Raohe ophiolite and its geological significance in Nadanhadaling [in Chinese with English abstract], *Heilongjiang Geol.*, *1*(1), 3–18.
Karig, D. E. (1983), Accreted terranes in the northern part of the Philippine Archipelago, *Tectonics*, *2*, 211–236, doi:10.1029/TC002i002p00211.
Klemd, R., T. John, E. E. Scherer, S. Rondenay, and J. Gao (2011), Changes in dip of subducted slabs at depth: Petrological and geochronological evidence from HP–UHP rocks (Tianshan, NW-China), *Earth Planet. Sci. Lett.*, *310*, 9–20.
Koglin, N., D. Kostopoulos, and T. Reischmann (2009), The Lesvos mafic–ultramafic complex, Greece: Ophiolite or incipient rift?, *Lithos*, *108*, 243–261.
Kojima, S. (1989), Mesozoic terrane accretion in Northeast China, Sikhote-Alin and Japan regions, *Palaeogeogr. Palaeoclimatol. Palaeoecol.*, *69*, 213–232.
Kojima, S., and S. Mizutani (1987), Triassic and Jurassic radiolarian from the Nadanhada range,northeast China, *Trans. Proce. Palaeontol. Soc. Japan New Ser.*, *148*, 256–275.
Kröner, A., et al. (2014), Reassessment of continental growth during the accretionary history of the Central Asian Orogenic Belt, *Gondwana Res.*, *25*, 103–125.
Le Bas, M. J. (2000), IUGS reclassification of the high-Mg and picritic volcanic rocks, *J. Petrol.*, *41*, 1467–1470.
Li, J. Y. (2006), Permian geodynamic setting of Northeast China and adjacent regions: Closure of the Paleo-Asian Ocean and subduction of the paleo-Pacific Plate, *J. Asian Earth Sci.*, *26*, 207–224.
Li, W. K., J. X. Han, S. X. Zhang, and F. Y. Meng (1979), The main characteristics of the Upper Palaeozoic stratigraphy at the North Nadanhada range, Heilongjiang Province [in Chinese with English abstract], *Bull. Chin. Acad. Geol. Sci.*, *1*(1), 104–120.
Liu, Y. S., Z. C. Hu, S. Gao, D. Günther, J. Xu, C. G. Gao, and H. H. Chen (2008), In situ analysis of major and trace elements of anhydrous minerals by LA-ICP-MS without applying an internal standard, *Chem. Geol.*, *257*, 34–43.
Liu, Y., Z. Hu, K. Zong, C. Gao, S. Gao, J. Xu, and H. Chen (2010), Reappraisement and refinement of zircon U-Pb isotope and trace element analyses by LA-ICP-MS, *Chin. Sci. Bull.*, *55*, 1535–1546.
Ludwig, K. R. (2003), ISOPLOT 3.00: A Geochronological Toolkit for Microsoft Excel. Berkeley: Berkeley Geochronology Center, California.
Maruyama, S. (1997), Pacific-type orogeny revisited: Miyashiro-type orogeny proposed, *Island Arc*, *6*, 91–120.
Meschede, M. (1986), A method of discriminating between different types of mid-ocean ridge basalts and continental tholeiites with the Nb–Zr–Y diagram, *Chem. Geol.*, *56*, 207–218.
Mizutani, S., and S. Kojima (1992), Mesozoic radiolarian biostratigraphy of Japan and collage tectonics along the eastern continental margin of Asia, *Palaeogeogr. Palaeoclimatol. Palaeoecol.*, *96*, 3–22.
Mizutani, S., J. A. Shao, and Q. L. Zhang (1989), The Nadanhada terrane in relation to Mesozoic tectonics on continental margins of East Asia [in Chinese with English abstract], *Acta Geol. Sin.*, *63*(3), 204–215.

Natal'in, B. A. (1991), Mesozoic accretion and collision tectonics of southern USSR Far East, *Pacific Geol.*, *10*, 3–23.
Natal'in, B. A. (1993), History and modes of Mesozoic accretion in southeastern Russia, *Island Arc*, *2*, 15–34.
Nelson, D. R. (1997), Compilation of SHRIMP U–Pb zircon geochronology data, 1996, *Geol. Survey West. Australia. 1997/2*, 189 pp.
Pearce, J. A. (2008), Geochemical fingerprinting of oceanic basalts with applications to ophiolite classification and the search for Archean oceanic crust, *Lithos*, *100*, 14–48.
Pearce, J. A., and J. R. Cann (1973), Tectonic setting of basic volcanic rocks determined using trace element analyses, *Earth Planet. Sci. Lett.*, *19*, 290–300.
Pearce, J. A., and M. J. Norry (1979), Petrogenetic implications of Ti, Zr, Y, and Nb variations in volcanic rocks. Contrib, *Mineral. Petrol.*, *69*, 33–47.
Pearce, J. A., and D. W. Peate (1995), Tectonic implications of the composition of volcanic arc magmas, *Annu. Rev. Earth Planet. Sci.*, *23*, 251–285.
Ren, J. S., B. G. Niu, and Z. G. Liu (1999a), Soft collision, superposition orogeny and polycyclic suturing [in Chinese with English abstract], *Earth Sci. Front.*, *6*(3), 85–93.
Ren, J. S., Z. X. Wang, B. W. Chen, C. F. Jiang, B. G. Niu, J. Y. Li, G. L. Xie, Z. G. He, and Z. G., Liu (1999b), The tectonics of China from a global view– A guide to the tectonic map of China and adjacent regions, *Geol. Pub. House, Beijing*, pp. 4–32.
Sengör, A. M. C., and B. A. Natal'in (1996), Paleotectonics of Asia: Fragments of a synthesis, in *The Tectonic Evolution of Asia*, edited by A. Yin and T. M. Harrison, pp. 486–640, Cambridge Univ. Press, Cambridge.
Sengör, A. M. C., B. A. Natal'in, and V. S. Burtman (1993), Evolution of the Altaid tectonic collage and Palaeozoic crustal growth in Eurasia, *Nature*, *364*, 299–307.
Shao, J. A., and K. D. Tang (1995), *Terranes in Northeast China and Evolution of Northeast Asia Continental Margin* [in Chinese], pp. 185, Seismic Press, Beijing.
Shao, J. A., C. Y. Wang, K. D. Tang, and Q. Y. Zhang (1990), The relationship between Nadanhada Range stratums and terrane [in Chinese with English abstract], *J. Stratigr.*, *14*(4), 286–291.
Shao, J. A., K. D. Tang, C. Y. Wang, Q. J. Zang, and Y. P. Zhang (1991), The tectonic characteristics and evolution of Nadanhada Terrane [in Chinese], *Sci. China*, *7*, 744–750.
Steiger, R. H., and E. Jäger (1977), Subcommission on geochronology: Conventionon the use of decay constants in geo- and cosmochronology, *Earth Planet. Sci. Lett.*, *36*, 359–362.
Stern, R. A., E. C. Syme, and S. B. Lucas (1995), Geochemistry of 1.9 Ga MORB- and OIB-like basalts from the Amisk collage, Flin Flon Belt, Canada: Evidence for an intra-oceanic origin, *Geochim. Cosmochim. Acta*, *59*(15), 3131–3154.
Stern, R. J. (2002), Subduction zones, *Rev. Geophys. 40*(4), 1012, doi:10.1029/2001RG000108.
Sun, S. S., and W. F. McDonough (1989), Chemical and isotopic systematics of oceanic basalts: Implications for mantle composition and processes, in *Magmatism in the Ocean Basins*, edited by A. D. Saunders and M. J. Norry, *Geol. Soc. London Spec. Publ.*, *42*, 528–548.
Taira, A. (2001), Tectonic evolution of the Japanese Island arc system, *Annu. Rev. Earth Planet. Sci.*, *29*, 109–134.
Taira, A., K. T. Pickering, B. F. Windley, and W. Soh (1992), Accretion of Japanese island arcs and implications for the origin of Archean greenstone belts, *Tectonics*, *11*, 1224–1244, doi:10.1029/92TC00597.
Tang, K. D. (1990), Tectonic development of Paleozoic foldbelts at the northern margin of the Sino–Korean craton, *Tectonics*, *9*, 249–260, doi:10.1029/TC009i002p00249.
Thompson, G., W. B. Bryan, and S. E. Humphris (1989), Axial volcanism of the East Pacific Rise, 10 -12N, in *Magmatism in the Ocean Basin*, edited by A. D. Saunders and M. J. Norry, *Geol. Soc. London Spec. Publ.*, 42, 181–200.
Wang, C. Y., B. X. Kang, and H. R. Zhang (1986), A discovery of Triassic nonodonts in the Nadanhada Range and the Geological significance, in *Contributions to the Project of Plate Tectonics in North China* [in Chinese with English abstract], edited by C. Y. Li, pp., 208–214, Geol. Publ. House, Beijing.
Wang, X. Z. (1959), Mesozoic marine strata in Raohe Mesozoic fold belt of northeastern China [in Chinese with English abstract], *Geol. Sci.*, *2*, 50–51.
Wiedenbeck, M., P. Alle, F. Corfu, W. L. Griffin, M. Meier, F. Oberli, A. V. Quadt, J. C. Roddick, and W. Spiegel (1995), Three natural zircon standards for U–Th–Pb, Lu–Hf, trace element and REE analyses, *Geostand. Geoanalyt. Res.*, *19*, 1–23.
Wilde, S. A., X. Z. Zhang, and F. Y. Wu (2000), Extension of a newly-identified 500 Ma metamorphic terrain in Northeast China: Further U-Pb SHRIMP dating of the Mashan Complex, Heilongjiang Province, China, *Tectonophysics*, *328*, 115–30.
Wilde, S. A., F. Y. Wu, and X. Z. Zhang (2003), Late Pan-African magmatism in Northeastern China: SHRIMP U-Pb zircon evidence for igneous ages from the Mashan Complex, *Precambrian Res.*, *122*, 311–27.
Williams, I. S. (1998), U–Th–Pb geochronology by ion microprobe, in *Applications of Microanalytical Techniques to Understanding Mineralizing Processes*, vol. 7, edited by M. A. McKibben, W. C. Shanks III, and W. I. Ridley, pp. 1–35, Rev. Eco. Geol., Littleton, Colo.
Winchester, J. A., and P. A. Floyd (1976), Geochemical magma type discrimination: application to altered and metamorphosed igneous rocks, *Earth Planet. Sci. Lett.*, *45*, 326–336.
Windley, B. F., D. V. Alexeiev, W. Xiao, A. Kröner, and G. Badarch (2007), Tectonic models for accretion of the Central Asian Orogenic Belt, *J. Geol. Soc. London.*, *164*, 31–47.
Wu, F. Y., D. Y. Sun, H. M. Li, B. M. Jahn, and S. A. Wilde (2002), A-type granites in Northeastern China: Age and geochemical constraints on their petrogenesis, *Chem. Geol.*, *187*, 143–173.
Wu, F. Y., J. H. Yang, C. H. Lo, S. A. Wilde, D. Y. Sun, and B. M. Jahn (2007), Jiamusi Massif in China: a Jurassic accretionary terrane in the western Pacific, *Island Arc*, *16*, 156–172.
Wu, F. Y., D. Y. Sun, W. C. Ge, Y. B. Zhang, M. L. Grant, S. A. Wilde, and B. M. Jahn (2011), Geochronology of the Phanerozoic granitoids in northeastern China, *J. Asian Earth Sci.*, *41*, 1–30.
Xiao, W. J., B. Windley, J. Hao, and M. G. Zhai (2003), Accretion leading to collision and the Permian Solonker suture, Inner Mongolia, China: Termination of the Central Asian Orogenic Belt, *Tectonics*, *22*(6), 1069, doi:10.1029/2002TC001484.
Xiao, W. J., B. F. Windley, G. Badarch, S. Sun, J. Li, K. Qin, and Z. Wang (2004a), Palaeozoic accretionary and convergent tectonics of the southern Altaids: Implications for the growth of Central Asia, *J. Geol. Soc. London*, *161*, 339–342.
Xiao, W. J., L. C. Zhang, K. Z. Qin, S. Sun, and J. Li (2004b), Paleozoic accretionary and collisional tectonics of the eastern Tienshan (China): Implications for the continental growth of Central Asia, *Am. J. Sci.*, *304*, 370–395.
Xu, J. W., G. Zhang, and W. X. Tong (1987), Formation and evolution of the Tancheng–Lujiang shear fault system: A major shear system to the northwest of Pacific Ocean, *Tectonophysics*, *134*, 273–310.
Yang, J. Z., H. J. Qiu, J. P. Sun, and X. Z. Zhang (1998), Juejinshan Complex and its tectonic significance, *J. Changchun Univ. Sci. Tec.*, *28*(4), 380–385.
Zhang, K. W., J. A. Shao, K. D. Tang, Q. Zhang, and X. Y. Li (1997), The geochemical characteristics and the geological significance of gree-cshists in Yuejinshan Group, *Acta Petrol. Sin.*, *13*(2), 168–172.
Zhang, Q., and G. Q. Zhou (2001), Ophiolites in China [in Chinese with English abstract], pp. 182, Science Press, Beijing.
Zhang, Q. L., and S. Mizutani (2004), From plate tectonics to terrane concept [in Chinese with English abstract], *Jiangsu Geol.*, *28*(1), 1–6.

Zhang, Q. Y. (1990), Triassic-Jurassic radiolarian fauna in Nadanhada of northeastern China. Bulletin of Shenyang Institute of Geology and Mineral Resources [in Chinese with English abstract], *Chin. Acad. Geol. Sci.*, *21*, 157–191.

Zhao, H. L., J. F. Deng, F. J. Chen, Q. Hu, and S. K. Zhao (1996), Petrology and tectonic setting of Middle Jurassic volcanic rocks in Wanda Mountain, Heilongjiang Province [in Chinese with English abstract], *Earth Sci. Rev.*, *21*(4), 428–432.

Zhou, J. B., and S. A. Wilde (2013), The crustal accretion history and tectonic evolution of the NE China segment of the Central Asian Orogenic Belt, *Gondwana Res.*, *23*, 1365–1377.

Zhou, J. B., S. A. Wilde, X. Z. Zhang, G. C. Zhao, C. Q. Zheng, Y. J. Wang, and X. H. Zhang (2009), The onset of Pacific margin accretion in NE China: evidence from the Heilongjiang high-pressure metamorphic belt, *Tectonophysics*, *478*, 230–246.

Zhou, J. B., S. A. Wilde, G. C. Zhao, X. Z. Zhang, H. Wang, and W. S. Zeng (2010a), Was the easternmost segment of the Central Asian Orogenic Belt derived from Gondwana or Siberia: an intriguing dilemma?, *J. Geodyn.*, *50*, 300–317.

Zhou, J. B., S. A. Wilde, G. C. Zhao, X. Z. Zhang, C. Q. Zheng, and H. Wang (2010b), New SHRIMP U–Pb Zircon ages from the Heilongjiang Complex in NE China: Constraints on the Mesozoic evolution of NE China, *Am. J. Sci.*, *310*, 1024–1053.

Zhou, J. B., S. A. Wilde, G. C. Zhao, X. Z. Zhang, C. Q. Zheng, and H. Wang (2010c), Pan-African metamorphic and magmatic rocks of the Khanka Massif, NE China: Further evidence regarding their affinity, *Geol. Mag.*, *147*(5), 737–749.

Zhou, J. B., S. A. Wilde, X. Z. Zhang, S. M. Ren, and C. Q. Zheng (2011a), Pan-African metamorphic rocks of the Erguna Block in the Great Xing'an Range, NE China: Evidence for the timing of magmatic and metamorphic events and their tectonic implications, *Tectonophysics*, *499*(1–4), 105–117.

Zhou, J. B., S. A. Wilde, X. Z. Zhang, G. C. Zhao, and F. L. Liu (2011b), A $>$1300 km late Pan-African metamorphic belt in NE China: new evidence from the Xing'an Block and its tectonic implications, *Tectonophysics*, *509*, 280–292.

Zhou, J. B., S. A. Wilde, F. L. Liu, and J. Han (2012a), Zircon U-Pb and Lu-Hf isotope study of the Neoproterozoic Haizhou Group in the Sulu orogen: Provenance and tectonic implications, *Lithos*, *136–139*, 261–281.

Zhou, J. B., S. A. Wilde, X. Z. Zhang, F. Liu, and J. H. Liu (2012b), Detrital zircons from Phanerozoic rocks of the Songliao Block, NE China: Evidence and tectonic implications, *J. Asian Earth Sci.*, *47*, 21–34.

Zhou, J. B., J. Han, S. A. Wilde, X. D. Guo, W. S. Zeng, and J. L. Cao (2013), A primary study of the Jilin-Heilongjiang high-pressure metamorphic belt: Evidence and tectonic implications, *Acta Petrol. Sin.*, *29*(2), 386–398.

Zyabrev, S., and A. Matsuoka (1999), Late Jurassic (Tithonian) radiolarians from a clastic unit of the Khabarovsk complex (Russian Far East): Significance for subduction accretion timing and terrane correlation, *Island Arc*, *8*, 30–37.